Fride Myhrvold

Synthesis and characterisation of hierarchical SAPO-5 employing sustainable meso-SDAs

Master's thesis in Chemistry
Supervisor: Karina Mathisen
Co-supervisor: Muhammad Mohsin Azim and Daniel Ali
December 2022

NTNU
Norwegian University of
Science and Technology

Fride Myhrvold

Synthesis and characterisation of hierarchical SAPO-5 employing sustainable meso-SDAs

Master's thesis in Chemistry
Supervisor: Karina Mathisen
Co-supervisor: Muhammad Mohsin Azim and Daniel Ali
December 2022

Norwegian University of Science and Technology
Faculty of Natural Sciences
Department of Chemistry

NTNU
Norwegian University of
Science and Technology

Acknowledgements

Summary

Hierarchical SAPO-5 was synthesised hydrothermally and with the use of the sustainable meso-SDAs glucose and sucrose. A parameter study was conducted to investigate the effect of addition order, crystallisation time and temperature on the synthesis, and all samples were characterised with XRD, nitrogen physisorption, ICP-MS, SEM and FT-IR analysis to evaluate the quality of the samples and their pore hierarchy. It was evident from characterisation that both synthesis addition orders studied produced samples with some degree of hierarchy. However, Synthesis A gave samples with higher relative crystallinity, higher BET surface area and smaller particle size, while Synthesis B promoted more mesopore volume and a higher degree of hierarchy. The parameter study showed that a longer crystallisation time reduced the Tridymite impurities and that introducing a low-temperature pre-crystallisation step increased the AFI phase for samples with Synthesis B using sucrose as the meso-SDA, and glucose proved to be superior for promoting acid sites in the material.

Sammendrag

Hierarkisk SAPO-5 ble syntetisert hydrotermisk og med bruk av de bærekraftige meso-SDAene glukose og sukrose. En parameterstudie ble utført for å undersøke effekten av tilsetningsrekkefølge, krystalliseringstid og temperatur på syntesen, og alle prøvene ble karakterisert med XRD, nitrogen fysisorpsjon, ICP-MS, SEM og FT-IR analyse for å evaluere kvaliteten på prøvene og deres porehierarki. Det var tydelig fra karakterisering at begge syntese tilsetningsrekkefølgene som ble studert ga prøver med en viss grad av hierarki. Syntese A ga prøver med høyere relativ krystallinitet, høyere BET-overflateareal og mindre partikkelstørrelse, mens Syntese B fremmet mer mesoporevolum og en høyere grad av hierarki. Parameterstudien viste at en lengre krystalliseringstid reduserte Tridymite-urenhetene og at innføring av et lavtemperatur-forkrystalliseringstrinn økte AFI-fasen for prøver med Syntese B og ved bruk av sukrose som meso-SDA, mens glukose viste seg å være overlegen for å fremme syre nettsteder i materialet.

Contents

Abbreviations

AFI   Aluminumphosphate FIve (framework)

Al-OH   Aluminium hydroxyl

Al_2O_3 Pseudo-boehmite

AlPO   Aluminumphosphate

BET   Brunauer-Emmet-Teller

BJH   Barret-Jayner-Holenda

CTAB   Cetyltrimethylammonium bromide

CO_2 Carbon dioxide

FT-IR   Fourier-Transform Infrared Spectroscopy

H_3PO_4 Ortho-phosphoric acid

HNO_3 Nitric acid

HTHP   High Temperature High Pressure

ICP-MS   Inductively Coupled Plasma- Mass Spectroscopy

IR   Infrared

IUPAC   International Union of Pure and Applied Chemistry

LN-MCT   Liquid Nitrogen cooled Mercury Cadmium Telluride

N_2 Nitrogen

NTNU   Norwegian University of Science and Technology

PDADMAC	Polydiallyldimethylammonium chloride
P-OH	Phosphorous hydroxyl
PSD	Pore Size Distribution
PXRD	Powder X-Ray Diffraction
SAPO	Silica-aluminophosphates
SDA	Structure Directing Agent
SEM	Scanning Electron Microscopy
SiO_2	Colloidal silica
Si-OH	Silicon hydroxyl
SSA	Specific Surface Area
TEA	Triethylamine
TPHAC	[3-(trimethoxysilyl)propyl]hexadecyldimethyl ammonium chloride
TSE	Tensile Strength Effect
wt.%	Weight percentage
XRD	X-Ray Diffraction
ZSM-5	Zeolite Socony Mobil–5
Å	Ångstrøm (10^{-10} m)

1 Introduction

One of the greatest challenges of our time is the looming threat of climate change, as our never-ending consumption of the resources of the planet leads to the emission of greenhouse gases. Billions of tonnes of carbon dioxide, methane and nitrogen oxide gases are emitted into the atmosphere each year [1], and researchers are therefore looking for a solution where the gases can be reused in the industry to produce useful chemicals. Zeolites and zeotypes have in recent years gotten a lot of attention as a solution to this problem, and these materials have been reported to be active in catalysis for capturing these greenhouse gases and converting them into chemicals that can be further utilised in the chemical industry [2, 3].

However, the synthesis of such high-quality materials is also a polluting factor and contributes to the already large emissions coming from the chemical industry. The chemical industry today is said to be responsible for about 10% of the global carbon dioxide equivalent emissions, which is equivalent to 5.6 gigatonnes of CO_2-eq [4]. In 2007, 19% of emissions from the industry in the UK came from the production of chemicals [5]. It has therefore never been more important to implement the principles of green chemistry [6], to reduce the impact the industry has on the environment and climate.

Two of these principles are addressed in this thesis, where solutions to reduce the emissions of toxic gasses such as nitrogen oxide gases, and the use of less hazardous and toxic reagents in the synthesis of the molecular sieve SAPO-5. SAPO-5 is a porous material with a wide range of applications in catalysis, and preparing SAPO-5 with a hierarchical pore system has been proven to improve the mass-transfer abilities and enhance the overall catalytic performance [7]. Toxic and hazardous chemicals are often used as templates for mesopores in synthesis to produce this hierarchical pore system, which produces nitrogen oxide gas when combusted. By substituting these chemicals with more sustainable options, the synthesis itself becomes greener and less toxic waste is produced to harm the environment.

In this thesis, the synthesis of hierarchical SAPO-5 will for the first time be attempted with the use of sustainable mesoporous templates like glucose and sucrose. Synthesis parameters such as addition order, crystallisation time and temperature will be studied for the hydrothermal synthesis of the material, and a thorough characterisation will be conducted to evaluate the samples synthesised.

2   Theory

2.1   Molecular sieves and zeotypes

Molecular sieves are a group of crystalline materials with pores of uniform size. They are known for their large surface area and adsorption abilities due to their porosity and are especially useful for size separation of chemicals due to the uniformly sized pore system [8]. Molecular sieves exhibit a wide range of applications as adsorbents, catalysts, ion-exchangers, environment material, life sciences, in nanotechnology and others [9]. Zeolites and zeotypes are two groups of inorganic microporous molecular sieves that have been studied considerably for their catalytic applications [10].

Here, zeolites are aluminosilicates containing aluminium and silicon tetrahedrally coordinated cations that are bonded together via oxygen bridges, in a three-dimensional porous framework [10]. Zeotypes, on the other hand, is a hypernym used to describe materials build on the same principle, however with other tetrahedrally orientated cations, such as phosphorus, titanium, gallium, germanium or bohr [10]. Silicoaluminophosphates for example, also called SAPOs, are a well-known family of zeotypes, composed of aluminium, phosphorus and silicon cations [11, 12]. There exists a magnitude of SAPO materials exhibiting various pore dimensions and frameworks which are numerically named according to their respective zeolite framework, as SAPO-n [13]. They are known for being thermally stable up to 900 K and their acidic properties due to the silicon in the framework give them catalytic abilities similar to zeolites [14].

2.2   SAPO-5 and its catalytic abilities

SAPO-5 is a silicoaluminophosphate with the AFI framework shown in Figure 2.1. The name of the framework AFI derives from **A**luminumphosphate **FI**ve (AlPO-5), which is a material with a similar structure to SAPO-5, however has no silicon. The AFI framework has a one-dimensional pore system containing 12-membered-rings in the [001] direction of the unit cell [13]. The unit cell is hexagonal and the pores are considered wide with dimensions of 7.3 x 7.3 Ångstrøm (Å) [7].

Compared to the neutral isostructural AlPO materials with alternating Al and P atoms, SAPOs have a net negative charge due to phosphorus being substituted with silicon [15]. When silicon is present in the structure and a net negative charge is created on the surface of the material and a proton can be bound to the oxygen
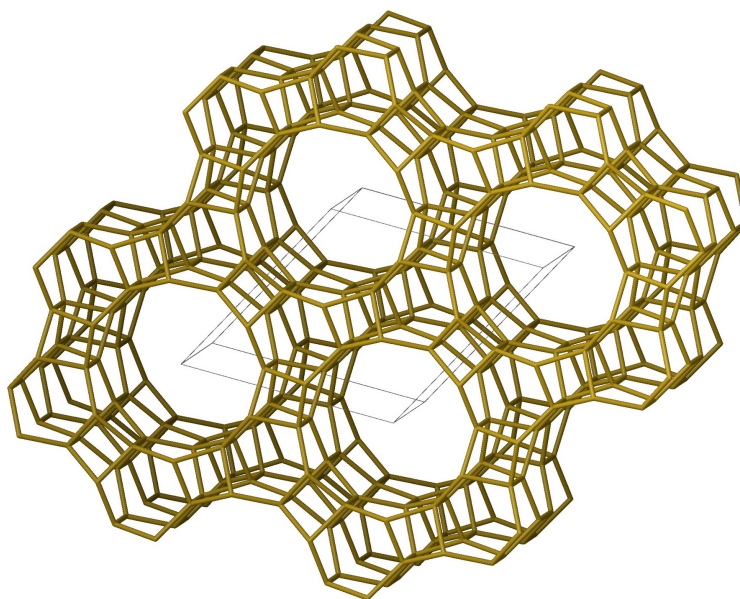
Figure 2.1: AFI framework of SAPO-5 illustrating the one-dimensional 12-membered-ring pore
system and the unit cell for the crystal structure [13].

next to the silicon cation in order to compensate for the charge imbalance, giving
rise to Brønsted-Acid sites as shown in Figure 2.2 [16]. This acidic feature of
SAPO is beneficial for metal introduction via ion-exchange where the proton on
the Brønsted site is substituted with a metal ion [17]. SAPO-5 is therefore an
ideal catalyst support material [18] and can be used in acid catalysis as the acidic
property provides stronger interactions with hydrocarbons [12]. The number of
Brønsted acid sites of a material is dependent on the amount of silicon and its
distribution in the structure, which amount is often referred to as the Si/Al ratio
of the material and is tunable in synthesis [19].
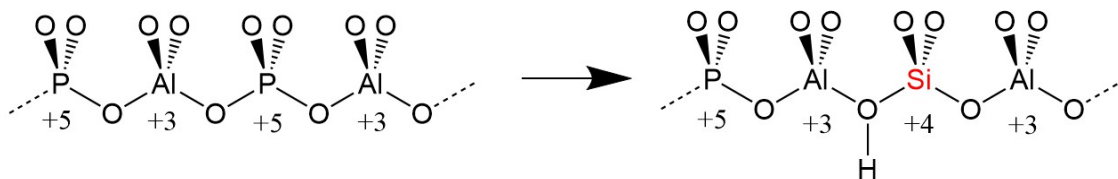
Figure 2.2: Illustrated on the left in the figure is the neutral framework of an AlPO, and on the
right is the negatively charged framework of a SAPO where a phosphorus atom is
substituted with a silicon atom creating the Brønsted-Acid site.

SAPO-5 has attracted significant attention in the industry for catalysis as it is active
in reactions such as the isomerization of xylene [20], the methanol to hydrocarbons
reaction [21], isopropylation of benzene [7], toluene alkylation by methanol [22] and
in the synthesis of cumene [23]. SAPO-5 is also known as a separator and in new
applications such as nonlinear optics and use as containers for carbon nanotubes

2

[24].

2.3   Synthesis of SAPO-5

There are several different ways to synthesise SAPO-5 such as microwave radiation, hydrothermal, solvothermal or ionothermal synthesis[12, 24–26]. Hydrothermal synthesis is a long studied and established synthesis technique [27] and was chosen for this thesis due to the abundant literature on the synthesis of hierarchical SAPO-5.

2.3.1   Hydrothermal synthesis

Hydrothermal synthesis is broadly defined as a chemical reaction between substances in a reaction medium of water (hydro-), where the aqueous solution is sealed and heated to temperatures from 100-1000°C (-thermal) with pressure from 10-1000 bar [27]. The synthesis usually involves sealing the aqueous solution in a specialised high-pressure autoclave, see Figure 2.3, where sub- or supercritical conditions of the solvent are reached [28]. The reaction mechanism of the crystallisation is complex and understanding of the specific mechanisms during crystallisation is lacking [9]. Compared to the mechanism of solid-state reactions where atoms diffuse onto the interface of the particles, hydrothermal synthesis involves reactions between the different ions and molecules in the solution [27].

Figure 2.3: Autoclaves used for hydrothermal synthesis, where a Teflon-lined container containing the gel solution is sealed inside the stainless steel autoclave followed by crystallisation in the oven.

A typical hydrothermal synthesis of zeotypes can be described in a few simple steps. First, the precursors and templates are mixed together into an aqueous solution and aged to a solution gel [29]. It is then transferred into the autoclave and heated to a desired temperature, where the reactants in the gel remain amorphous for some time [28]. After an induction period, crystalline material is produced, and if successful,

all the amorphous material will eventually be replaced with the same amount of crystalline material [27]. The product is retrieved by washing and drying the sample [9]. A general description of the crystallisation mechanism from a solution involves nucleation of the desired phase and growth to larger particles [30]. For zeotypes this can be described as the dissolving of the amorphous gel as the reagents are consumed by the growth of crystals [9].

2.3.2   Structure directing agents

Structure directing agent (SDA), often referred to as template, are chemicals used in the synthesis of porous materials to direct the formation of the pore system. They are typically chemicals made of a nonpolar, hydrophobic hydrocarbon tail and a polar hydrophilic head group [31]. While there are different types of SDAs, such as inorganic cations like sodium, this thesis will focus on organic cations such as organic ammonium, which direct the assembly pathway and fill the pore space [32]. The formation mechanism of zeotypes can be described as the arrangement of the SiO_4, AlO_4 and PO_4 tetrahedra around the positively charged SDA using Van Der Waals interactions [10]. Some examples for such organic ammoniums are cyclohexylamine [7], Tri-n-propylamine, 2-diethylethanolamine, tetrapropylammonium hydroxide [11] and Triethylamine (TEA) [11, 21] which can be used as a template for the micropores in SAPO-5.

The examples above are referred to as micro-SDA as these create micropores, however other SDAs can be used to create pores of other dimensions such as mesopores. These so-called meso-SDAs work in the same way as the organic cation micro-SDA and the crystalline is arranged around the meso-SDA [33]. Materials with mesopores have successfully been synthesised with different meso-SDAs, e.g. quaternary ammonium surfactants like cetyltrimethylammonium bromide (CTAB), see Figure 2.4 [34], organosilanes like [3-(trimethoxysilyl)propyl]hexadecyldimethyl ammonium chloride (TPHAC) [7] and polymers like polydiallyldimethylammonium chloride (PDADMAC) [34].
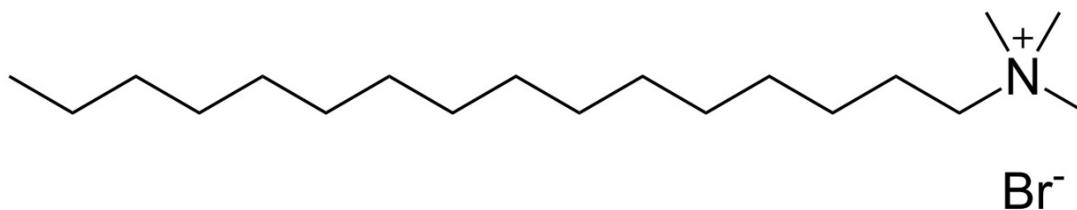
Figure 2.4: Chemical structure of the quaternary ammonium surfactant C-TAB which is often used as a meso-SDA for hierarchical materials.

Using organic SDA as described above to produce pore systems in materials is beneficial as the size, shape and morphology of the pores can be directly controlled by the type of SDA used [29]. Finally, to remove the template after crystallisation, a calcination step is added where the material is heated at high temperatures to combust the organic material, resulting in a porous material that is kinetically stable at high temperatures [27, 32, 33].

2.4   Hierarchical materials improving catalytic ability

Porous materials are classified by the International Union of Pure and Applied Chemistry (IUPAC) according to the size of the pores, where microporous materials have pores with a width of less than 2 nm, mesopore materials exhibit pore diameter from 2 nm up to 50 nm and macroporous materials have pores larger than 50 nm in diameter [35]. Conventional zeolites and zeotypes such as SAPO-5 are considered microporous, and as described above have numerous advantages for catalysis. However, there are some limitations to pure-microporous systems, such as diffusion limitations, short catalyst life-span and coke formation inside the micropores [34]. By introducing a secondary pore system into the materials, such limitations can be avoided as the larger pores are thought to function as diffusion highways and contribute to the mass transfer of chemicals throughout the material [36]. These new materials are defined as hierarchical materials and contain at least two levels of pore diameters, with microporous channels less than 2 nm and additional mesoporous and/or macroporous channels [10, 37].

The diffusitivity of a catalyst is important as it determines how many active sites on the material's surface area are utilised for catalytic reactions [38]. A material with narrow micropores experiences low molecular diffusion as the transport of reactants and products to and from the active sites is reduced when molecules have a similar size to the pore width. This is illustrated in Figure 2.5.A where the microporous material experiences a drop in the reactant concentration through the middle of the particle as diffusion is low. This delay in transport can result in the formation of undesired by-products which can account for coke formation that blocks the micropores. This leads to the deactivation of parts of the material as illustrated in Figure 2.5.B and a shorter catalyst lifespan as only the outer part of the material particle is active in catalysis and the interior part remains inactive [34].

Hierarchical zeolites, usually with secondary porosity in the mesoporous range, display an improved catalytic performance when compared to microporous zeolites due to the higher diffusion of larger particles within the mesopores to the active

sites in the zeolite without impediment, illustrated by the constant concentration of reactants through the particle in Figure 2.5.A [36, 37]. Diffusion throughout the zeolite particle is improved and a longer catalyst lifespan is achieved as the entire particle takes part in the reaction, see Figure 2.5.B and the catalyst experiences less coke formation [34].
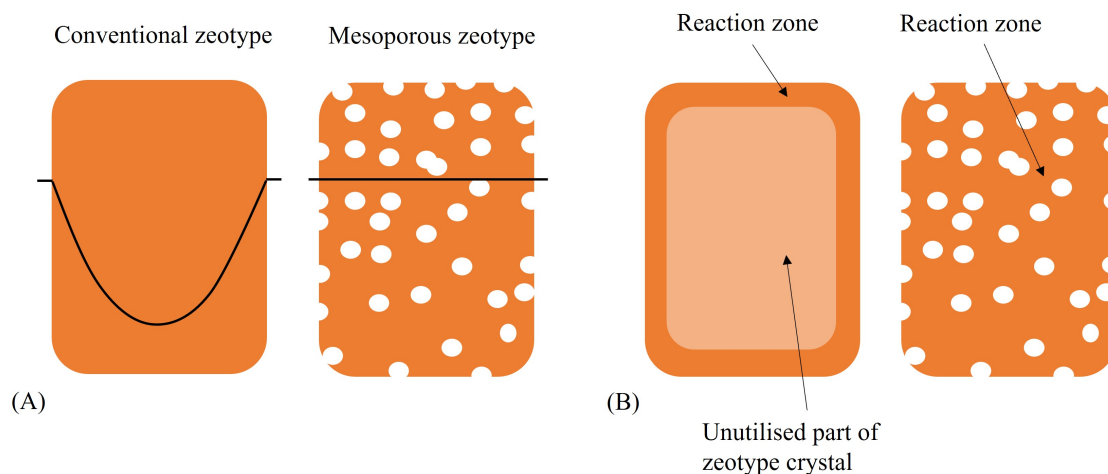
Figure 2.5: Schematic illustration of (A) the concentration profile of a reactant and (B) reaction zone for a (conventional) microporous and (mesoporous) hierarchical material, illustration adapted from Christensen et. al. [36].

Another important factor for hierarchical zeolites is the connectivity of the levels of pores, thus further improving diffusion. Interconnected micropores and mesopores refer to when the mesopores are connected to the micropores in different dimensions resulting in a shortening of the diffusion length as shown in Figure 2.6.c where the red pores represent mesopores, and mesopores being accessible from the outside of the zeolite particle [39]. A shortened diffusion length minimises the deactivation of the particle as the micropores are cut short by passing mesopores resulting in less coke-formations [34]. Without this connectivity as illustrated in Figure 2.6.d, diffusion length is not shortened and diffusion limitations are not necessarily improved as a shorter diffusion length is required to improve the performance of the catalyst [39].

There are two ways of obtaining hierarchical materials, either by creating intracrystalline mesopores inside the microporous structure or by introducing intercrystalline mesopores as voids in between nanosized microporous crystals as illustrated in Figure 2.6.b [37]. The former of the two can be obtained by soft-templating which is a bottom-up approach used to introduce a secondary pore system in the material [10, 34]. The soft template approach is described as a template-assisted synthesis

that uses meso-SDA like surfactants, organosilanes, or macro-molecular polymers to direct the formation of mesopore systems [10, 40]. This is often referred to as dual templating as both a micro- and meso-SDA take part in synthesis, where soft templates direct the formation of mesopores while micro-SDA directs the formation of microporous material around [40]. Hierarchical zeolites have been reported to enhance the diffusion rate three orders of magnitude compared to pure microporous material and have shown great promise in diffusion studies with n-heptane, 1,3-dimethylcyclohexane and n-undecane [39]. However, dual templating has also been reported to lead to the formation of a mixture of amorphous mesophase and crystalline microporous zeolites reducing the diffusion [40].
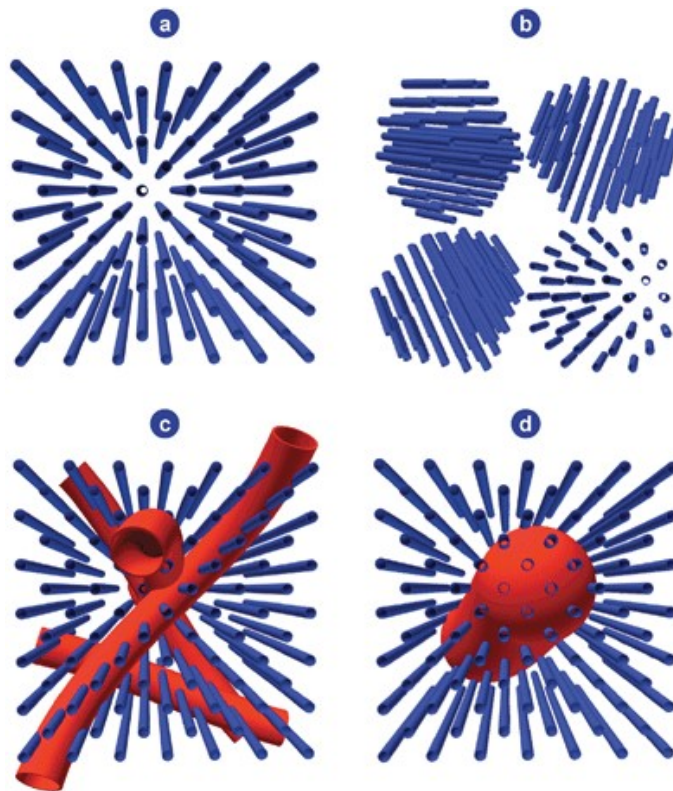
Figure 2.6: Schematic illustration of interconnectivity resulting in shorter diffusion length in micropores, where (a) represents a pure micropore material, (b) represents inter-crystalline mesopores in between nanosized microporous crystals, (c) represents interconnected micro- and mesopores and (d) represents a mesopore that is not interconnected to the micropores not resulting in a shorter diffusion length. Reproduced from Pérez-Ramírez et. al. [39] wth permission from the Royal Society of Chemistry.

2.4.1 Sustainable meso-SDAs

The quaternary ammonium and organosilanes surfactants used to produce mesopores in soft-templating are usually classified as toxic chemicals that are harmful to the environment, as well as being expensive and unsustainable [41]. The calcination

step conducted to remove these organic templates from the inorganic crystalline material results in the release of harmful gases such as hazardous nitrogen oxide gas (NOx) and greenhouse gases like carbon-dioxide (CO_2) as the chemicals are combusted [10, 32]. Chemical waste produced in the synthesis of hierarchical materials contains these chemicals and without proper waste treatment can end up directly damaging the environment.

As an attempt to avoid the use of such toxic chemicals in synthesis, more sustainable meso-SDAs can be utilised for soft-templating. Biomaterials like saccharides such as glucose, sucrose, starch and cellulose [42], have been reported to work as templates for mesopores in hierarchical zeolites and zeotypes. Although CO_2 is still produced when combusted, these alternative chemicals result in less damage to the environment from toxic waste and NOx gas production. In addition to being cheap materials compared to conventional meso-SDAs, they are commonly natural-derived and can be used to tune the size of the mesopores by choosing the saccharide with a desirable width. The chemical structure of glucose and sucrose are given in Figure 2.7, which were the two saccharides chosen for this thesis.
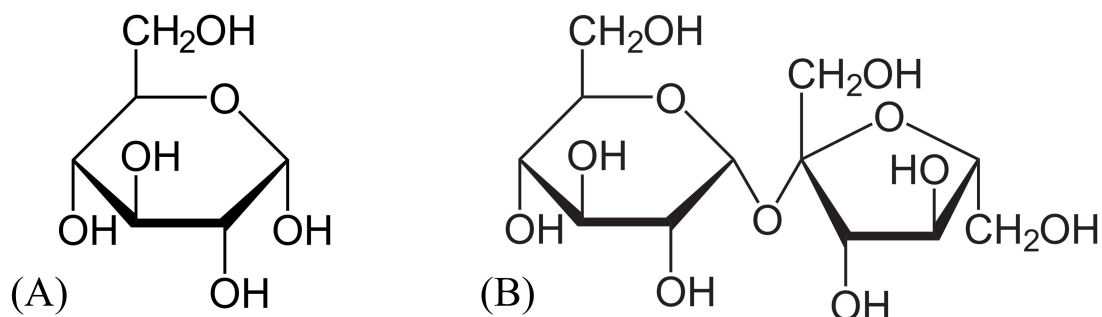
Figure 2.7: Chemical structure of glucose (A) and sucrose (B).

These sustainable meso-SDAs have shown great promise in the synthesis of hierarchical ZSM-5 zeolites, where sucrose produced a material with narrow mesopore distribution of 7 nm, exhibiting a superior catalytic activity in the methylation of 2-methylnaphtalene [43]. Nandan et al. introduced glucose as the meso-SDA for the synthesis of hierarchical ZSM-5 where the hierarchical porosity was enhanced simply by increasing the amount of glucose [44]. Saccharides have also been used as meso-SDA for zeotypes where Liu et. al. prepared hierarchical SAPO-11 with sucrose [45], Yang et. al. studied the synthesis effects of using glucose, sucrose and starch to produce hierarchical AlPO-5 [46] and Mariatti et. al. attempted the preparation of hierarchical SAPO-5 using monosaccharides from tomato plants [47].

2.5 Characterisation methods

Different characterisation methods were used to investigate the structure and properties of the hierarchical SAPO-5 samples, such as X-ray Diffraction, Nitrogen Physisorption, Inductively Coupled Plasma - Mass Spectroscopy, Scanning Electron Microscopy and Fourier-Transform Infrared Spectroscopy. In the following chapter, theory of each characterisation technique is presented.

2.5.1 X-ray diffraction (XRD)

X-ray diffraction (XRD) is a characterisation technique used to identify the crystalline phase of materials and give information about the atomic and molecular structure and phase purity [38]. The principle behind the technique is to radiate the sample with monochromatic X-rays that will interact with the crystal structure and scatter out in different angles depending on the crystal structure and chemical composition [48]. X-rays are electromagnetic radiation with wavelengths around 1 Å, and monochromatic X-rays are produced when a beam of electrons strikes a metal target, usually copper (Cu). Here, a $K\alpha$ transition occurs as an electron in the $1s$ shell of the Cu atom is ionised allowing an electron in the $2p$ shell to drop down and occupy the vacant space in the $1s$. This $K\alpha$ transition results in the release of energy as a monochromatic X-ray with a fixed wavelength of 1.5418 Å [29, 38].

The monochromatic X-rays are then radiated upon the sample and are scattered by the atoms in the crystal lattice. The reflected X-rays will scatter in directions depending on the structure and composition [38], and will preferably exhibit the same energy as the incident X-ray [29]. When the reflected X-rays are in-phase and interfere constructively, Bragg's law is satisfied as shown in Figure 2.8. Bragg's law is given by

$$2d \sin(\theta) = \text{n}\lambda \tag{2.1}$$

where d refers to the perpendicular distance between two planes in the crystal lattice, θ is the incident angle, also called Bragg angle, λ is the wavelength of the X-ray radiation and n is an integer number [29, 38]. Constructive interference is only possible if there are multiple of wavelengths from multiple solutions of the Bragg's law for n = 1, 2, 3, etc. and will occur at maximum intensity [48].
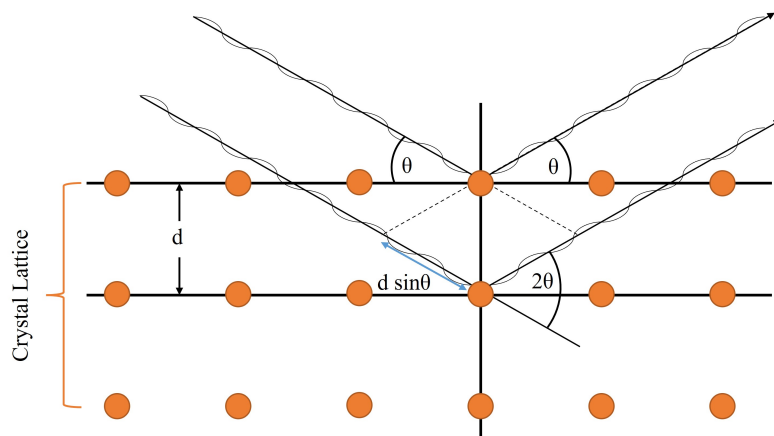
Figure 2.8: Illustration adapted from Niemantsverdriet et. al.[38], showing a monochromatic X-ray beam radiating into the crystal lattice and reflects out in-phase X-rays, where d is the distance between the crystal planes and θ is the angle between the beam and the crystal plane.

Powder X-ray Diffraction (PXRD) is used for analysing powdered samples, where the monochromatic beam radiates a finely powdered sample with randomly orientated crystals and lattice planes [29]. The intensity of each constructive interference X-rays is detected by a detector, and a diffractogram is produced where the intensity is plotted against 2θ. This diffractogram is unique for each material and can therefore be used as a "fingerprint" for identification [29]. A phase pure SAPO-5 sample would have a diffractogram as shown in Figure 2.9, which represents the AFI framework. For crystalline materials such as zeotypes, sharp reflections are present in the diffractogram, where each reflection represent a different d-spacing of the unit cell [38].
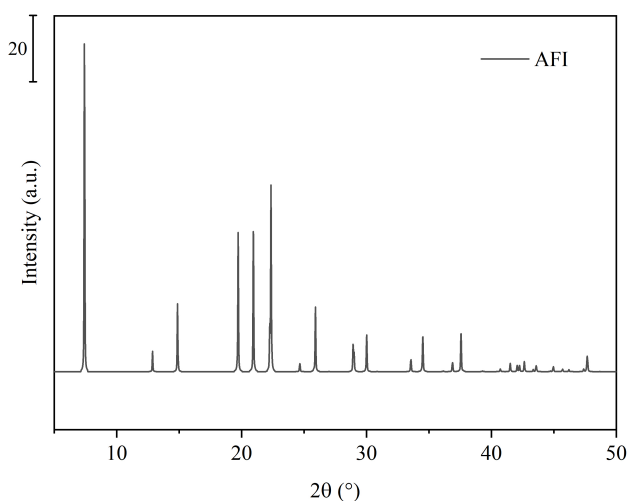
Figure 2.9: AFI diffractogram, data for graph collected from Database of Zeolite Structures[13].

10

The relative crystallinity of a series of samples can be found by using one sample as a standard to compare with the other samples. In this thesis, the conventional SAPO-5 was used as the standard, and the area under reflections at 7.5°, 14.9°, 19.8°, 21.1°, 22.5° and 26.0° [12] was used to calculate the crystallinity. The areas found were used to find the relative crystallinity according to this equation:

$$\%\text{Crystallinity} = \left(\frac{\text{Area under reflections on sample}}{\text{Area under reflections of standard}} \right) \times 100 \qquad (2.2)$$

Relative crystallinity will give an indication of the crystallinity of the desired phase exhibited by the standard sample and does not give information on the potential impurities or other phases present in the sample. One can have a sample with 100% crystallinity that also exhibits impurities, so it is important to use the diffractogram in the analysis as well. Relative crystallinity is not comparable with literature as the standard sample used is different from each project. The standard sample chosen for evaluation does not necessarily represent a typical diffractogram for all SAPO-5 materials and the technique can therefore only be used to compare one's own samples.

2.5.2 Nitrogen physisorption (BET/BJH)

Nitrogen physisorption is a technique that can be used to evaluate the surface area of a material. Physisorption refers to when a gas (adsorptive) comes in contact with a surface (adsorbent), usually solid, and they are bonded physically rather than chemically as in chemisorption. The forces involved in the bonding are usually London dispersion forces and short-term intermolecular repulsion forces [49]. The amount of gas adsorbed on the adsorbent is strongly correlated to the equilibrium pressure and temperature of the system, where the adsorption of gas increases with increasing pressure and decreasing temperature [50]. This relationship can be utilised to investigate the surface area and pore distribution of the solid material. The Brunauer-Emmet-Teller (BET) method and Barret-Joyner-Halanda (BJH) model use this relationship, where BET can be used to find the specific surface area (SSA) of the material and BJH gives the pore size distribution (PSD) [50, 51].

A physisorption isotherm is known as the relationship between the quantity of adsorbed gas and the equilibrium pressure of the gas at a constant temperature, and its shape can give information about what pores are present in a material. Most physisorption isotherms can be classified by eight different types that have been defined by the IUPAC [52] and De Gruyter [51], see Figure 2.10.
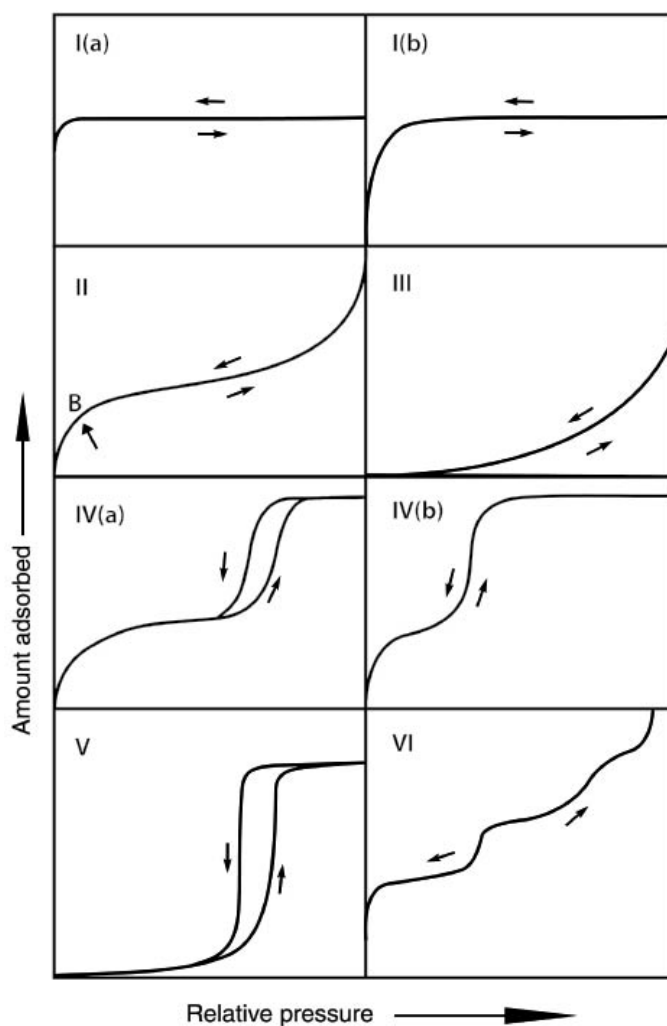
Figure 2.10: The eight different physisorption isotherms.   Reproduced with permission ©IUPAC, De Gruyter, 2015 [51].

Type I are typical for microporous materials with relatively small external surface areas, exhibiting a distinct plateau and limiting uptake determined by the accessible micropores [49]. Type I(a) is common for materials with narrow micropores, while type I(b) materials have a broader PSD with wider micropores and narrow mesopores [51]. This isotherm is expected from conventional microporous SAPO-5. Type II is given by nonporous or macroporous materials with a significant overlap of monolayer coverage, and type III isotherm is not common, usually found for nonporous carbon. Type IV is associated with capillary condensation due to mesopores featuring a final saturation plateau, and is typical for most mesoporous materials. Type IV(a) exhibits the characteristic hysteresis loop as the mesopores are wider than 4 nm while materials with smaller mesopores typically exhibit isotherm IV(b). Type V is also uncommon while type VI indicates step-wise adsorption on a uniform nonporous material [49, 51, 52]. The expected isotherm for the potential hierar-

chical SAPO-5 synthesised in this thesis would be a mix between isotherm I and IV(a).

The BET method is an isotherm model that can find the SSA of a material defined as the entire surface of a sample divided by its mass [52]. It uses a mathematical model to find the total amount of adsorbed gas molecules at monolayer coverage [49]. The principle behind the method is that a N_2 molecule occupies 0.162 nm^2 at 77 K, and knowing the amount of molecules adsorbed at monolayer coverage can give the total surface area of the material [53]. In literature, conventional SAPO-5 has been reported to exhibit a BET surface area from 204-417 m^2/g [20, 54], while hierarchical SAPO-5 has been reported to have BET surface area from 257-367 m^2/g [7, 21].

The t-plot, developed by Lippins, Linsen and de Boer, can be used to investigate the types of pores present in the material and quantify the volume and area of micropores [50]. It plots the amount of adsorbed gas against the thickness of the multilayer [52], where the interception of the y-axis can determine the volume of micropores present and the shape of the curve can determine whether the pores are micro- or mesopores [50]. Mesopore volume can be calculated by subtracting the micropore volume from the total pore volume.

When a material contains mesopores, hysteresis loops appear in the isotherms as a result of capillary pore condensation when the pores are filled with nitrogen [53]. Adsorption hysteresis occurs when the adsorption and desorption curves deviate from each other, and IUPAC has classified them into six different types that are identified with specific pore structures, as shown in Figure 2.11 [51, 52]. Type H1 represents a material with a narrow distribution of relatively uniform mesopores, while in H2 a more complex pore structure is common for materials where network effects are important. Type H2(a), common for silica gels, exhibits a steep desorption branch due to pore-blocking in a narrow range of pore necks while H2(b) is associated with a larger PSD [51]. Type H3 is not desired outcome from analysis as it represents poorly defined mesopores and does not reach any limiting adsorption at high pressures and is typically seen for materials like clay [49, 52]. Type H4 is similar and both types usually describe aggregates of plate-like particles that exhibit slit-shaped pores [52]. Type H4 is typical for aggregated crystals of zeolites, mesoporous zeolites, and micro-mesoporous carbons [51] and would therefore be expected for the hierarchical SAPO-5 samples. Type H5 is uncommon and is associated with pores containing open and partially blocked mesopores [51].

To investigate the PSD for samples, the BJH model can be applied, which uses
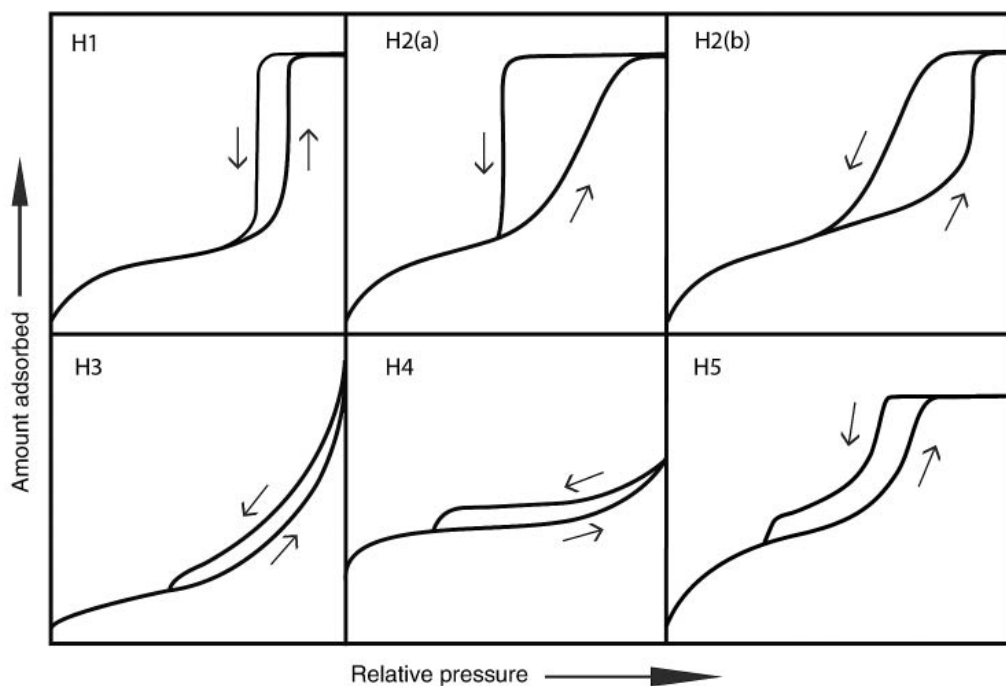
Figure 2.11: The six different types of hysteresis loops. Reproduced with permission ©IUPAC, De Gruyter, 2015 [51].

the phenomenon of capillary condensation described by the Kelvin equation. The concept of the procedures in this model is based on the emptying of the mesopores by a step-wise reduction of relative pressure [49]. The derived pore size distribution is usually illustrated by relative pore volume plotted against pore width [52] and can be used to find well-defined pore widths of mesopores in the structure by analysing the shape and location of peaks on the distribution curve. A known misconception with PSD is the tensile strength effect (TSE) which can appear as a peak at 3.8 nm in the distribution, most commonly in the desorption branch as the hysteresis loop is forced to close [55]. As microporous SAPO-5 does not contain mesopores, a flat distribution curve is expected, however for hierarchical samples made with meso-SDA, a peak should appear in the distribution curve as the template would provide uniform mesopores [21].

2.5.3   Inductively coupled plasma - mass spectroscopy (ICP-MS)

Inductively coupled plasma - mass spectroscopy (ICP-MS) is a characterisation technique known for being a rapid trace-element analysis giving precise and reliable results on both qualitative and quantitative information of species in a material [56]. In analysis, strong acids solutions are used to dissolve the sample, to atomic elements which are further ionized by inductively coupled plasma [57]. A detector in the mass spectroscope collects information on the elemental composition of the

species, determined by the signal based on the mass to ionic charge ratio for each element [56] in which the elements are detected by their specific atomic weight [58]. In this thesis, ICP-MS was used to evaluate the composition of building blocks in the samples and their molar ratios.

2.5.4 Scanning electron microscopy (SEM)

Electron microscopy is a versatile technique giving information on morphology, structure and composition of compounds in a wide range of magnifications [30, 38]. The principle behind electron microscopy is to emit electrons onto the sample with an electron gun called a tungsten filament, where the electrons are accelerated through a high voltage [29]. To obtain an image, electrons are focused either by an electrostatic or magnetic field, which is provided by lenses in the microscope.

Scanning electron microscopy (SEM) is used to study texture, topography and surface features of solid surfaces providing information on size, shape and composition, where the depth of focus results in definite 3D images [30]. SEM can be used for imaging in a magnification range covering 10^{-2}-10^2 µm. In SEM, electrons are accelerated through 5-50 keV and focused on a small area around 5-50 nm in diameter where the electrons scan the surface of the sample with a penetration depth up to 1 µm as shown in Figure 2.12.
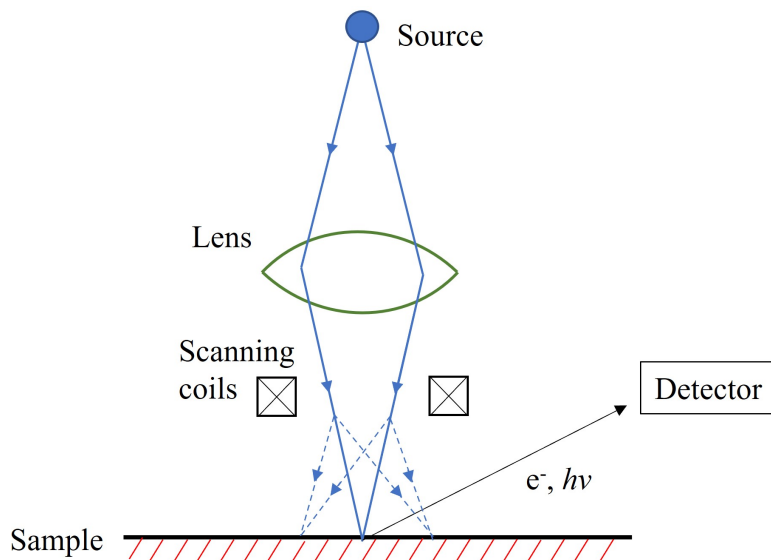
Figure 2.12: Principle behind SEM technique, where an electron beam, emitted from the electron source, passes through a lens and then scans the surface of the sample and electrons are re-emitted and detected by a detector. Illustration adapted from West [29].

After the electron beam interacts with the surface of the sample, particles and radi-

ation with different energies arise and can be detected, where back-scattering electrons and secondary electrons are used to record images [38]. Secondary electrons occur from the adsorption and re-emission of the electrons [29] and are recorded by a detector as shown in Figure 2.12.

If a sample is nonconductive, like metal-oxides, it needs to be coated with a thin layer of a conductive material, usually carbon or gold, to prevent the build-up of charge on the surface of the sample [29]. Hydrothermally synthesised SAPO-5 is reported in literature to present as spherical particles with a diameter of 20-30 µm [11, 20, 21], and are often described as agglomerates of thin crystalline rod-like particles [21] or platelets of around 100nm [7], however plate-like hexagonal crystals can be produced caused by the Si atoms [12].

2.5.5 Fourier-transform infrared spectroscopy (FTIR)

Infrared (IR) spectroscopy is a type of vibrational spectroscopy that can measure the vibrational energies of bonds in a compound, usually recorded in terms of the wavenumber (cm^{-1}). It is a technique that can characterise the strength and stiffness [18]. A molecular bond can vibrate in four different and independent ways: stretch vibrations, bending vibrations, both out of plane and in one plane, and torsion vibrations. These vibrations are again divided into symmetric and asymmetric vibrations [38]. The vibrations give rise to the degrees of freedom of a molecule, where a linear molecule with N atoms has 3N-5 fundamental vibrations while a non-linear has 3N-6 [38]. For instance, a non-linear molecule with three atoms like H_2O has three normal modes of vibration.

Transmission IR spectroscopy is one of the most common techniques used, where a thin wafer of around 10-100mg of sample is mounted in a way so the IR beam is transmitted through the sample [38]. When the compound is exposed to IR radiation, photons in the beam can excite the molecules to a higher vibrational level and some wavelength of light is absorbed [29]. The bonds excited to a higher vibrational level depend on the molecular structure of the compound and are collected by a detector [59]. The wavelengths measured in IR spectroscopy have frequencies in the mid-infrared range from 200-4000cm^{-1} [38].

The region from 3200-3900 cm^{-1} is known as the O-H bond region where different OH bonds can be detected on the SAPO-5 spectrum [60], see Figure 2.13.
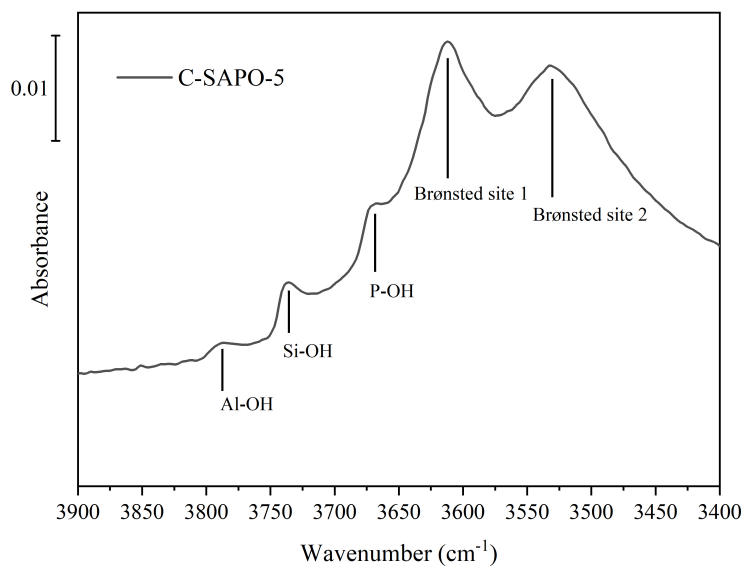
Figure 2.13: FTIR spectra of part of the OH-region of a calcined SAPO-5 taken at 300°C, showing bands for Brønsted sites at 3520 and 3625 cm^{-1} and P, Si and Al hydroxyls at 3680, 3740 and 3800 cm^{-1} respectively.

Hedge et. al reported the three peaks at 3680, 3740 and 3800 cm^{-1} as the external surface hydroxyls on SAPO-5 [15], where Schuth et. al. identified the bands P-OH, Si-OH and Al-OH hydroxyls respectively [60]. More specifically, 3675-80 cm^{-1} belonging to P-OH, bands around 3740-50 cm^{-1} belonging to Si-OH from impurities or in SiO$_2$ domains of the crystal, and bands at 3790 belong to Al-OH hydroxyls [60]. The bands at 3625 and 3520 cm^{-1} refer to Brønsted acid sites on the Al-OH-Si groups [60], whereas the first refers to the hydroxyl groups in the 12-membered ring of SAPO-5 and the latter is the acid sites in the 6-membered ring of the crystalline structure, according to literature [15, 60].

17

3   Experimental

The goal of this thesis was to study the hydrothermal synthesis of hierarchical SAPO-5 using sustainable meso-SDA. Conventional SAPO-5 inspired by the article by Ali et. al. [21] was initially synthesised and used as a standard for the hierarchical samples synthesised using meso-SDA of glucose and sucrose. A parameter study was done to evaluate how meso-SDA/Al ratio, synthesis addition order of precursors and template, crystallisation time and temperature affected the synthesis of hierarchical SAPO-5 using sustainable meso-SDA.

3.1   Chemicals

The aluminium, phosphorus and silica precursors were the same for all synthesises, with the exception of the silica precursor, where a chemical with a lower weight percentage was used for the last experiment. They were Pseudo-boehmite (Al_2O_3, 75 wt.%, Salsol), Ortho-phosphoric acid (H_3PO_4, 85 wt.%, Merck) and Colloidal Silica (SiO_2, 40wt.% and 30wt.%, Sigma-Aldrich) respectively. The micro-SDA used for all the synthesis was Triethylamine (($C_2H_5)_3$N, >99.5%, Sigma-Aldrich) and the meso-SDAs that was used were D-(+)-Glucose ($C_6H_{12}O_6$, ≥99.5%, Sigma-Aldrich) and D(+)-Saccharose (sucrose) ($C_{12}H_{22}O_{11}$, ≥99.5%, Sigma-Aldrich).

3.2   Synthesis of conventional SAPO-5

The procedure of the hydrothermal synthesis of conventional SAPO-5 was inspired by Ali et al. [21] where a material with molar compositions given in Equation 3.1 was produced.

$$1.0 \text{ Al} : 1.0 \text{ P} : 0.2 \text{ Si} : 0.6 \text{ TEA} : 30 \text{ H}_2\text{O} \tag{3.1}$$

First 8.48 g of H_3PO_4 was mixed with 39.75g of distilled water, and 5.00 g of Al_2O_3 was added and stirred for 2 hours. Then 2.21 g of SiO_2 was added and stirred for 45 minutes, followed by adding 4.47 g of TEA dropwise. The gel solution was then aged for 30 minutes while stirring, and then added to a stainless steel Teflon-lined autoclave that was placed in the oven for crystallisation at 200°C for 24 hours.

After the autoclave was cooled in air, the product was washed four times with 150 mL distilled water in a centrifuge for 10 minutes each time at 1500 rpm. The product was then dried in the oven for 72 hours at 70°C in air, and calcined for 5 hours at 600 °C with a ramp rate of 1°C/min.

3.3 Synthesis of hierarchical SAPO-5

The synthesis of hierarchical SAPO-5 using sustainable meso-SDAs has not been studied in great depth, and a parameter study was therefore conducted to investigate the effect of synthesis parameters. The variables that were chosen to study were the type of meso-SDA, the molar ratio of meso-SDA to Al, addition order, crystallisation time and crystallisation temperature. A series of experiments were conducted to look at the effect of each variable, and the procedure and reasoning for each experiment were described in the following chapters. The amount of each precursor and template used for all hierarchical samples was calculated from the theoretical molar ratio given in Equation 3.2.

$$1.0 \text{ Al} : 1.0 \text{ P} : 0.2 \text{ Si} : 0.6 \text{ TEA} : X \text{ Meso-SDA} : 30 \text{ H}_2\text{O} \qquad (3.2)$$
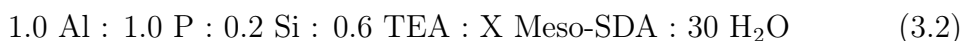
3.3.1 Experiment investigating addition order

For this experiment, the effect of changing the reactant addition order was investigated using two different synthesis addition orders. Specifically, the meso-SDA was added either after or before the phosphorus precursor referring to Synthesis A and B, respectively. Both glucose and sucrose were used for meso-SDA, and the amount added varied from 0.025-0.1 molar ratio for all series with the exception of glucose with synthesis A, where the amount varied from 0.025-0.3 to investigate any trends in a longer series. All samples in this experiment were crystallised for 24 hours at 200°C and calcined at 550°C.

The first synthesis was the same that was used for the conventional SAPO-5 inspired by Ali et. al.[21] where the general procedure and the reaction environment were the same as for conventional, except for the addition of sustainable meso-SDA. The meso-SDAs were dissolved in 10 g of distilled water that was subtracted from the original water that was mixed with the phosphoric acid to maintain the water molar ratio of the gel solution. The meso-SDA solution was added dropwise to the gel after the addition of TEA. This synthesis was named **Synthesis A**, as the meso-SDA was added **after** the ortho-phosphoric acid illustrated in Figure 3.1, and the samples were marked with an **a** on the start of the sample name.
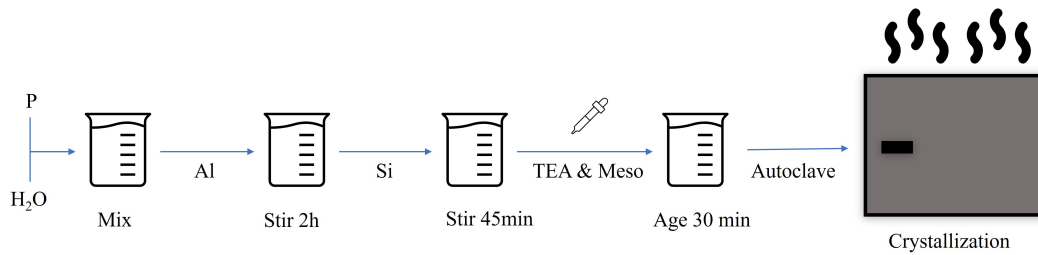
Figure 3.1: Schematic illustration of Synthesis A inspired by Ali et. al.[21]

The second synthesis carried out was inspired by Mariatti et. al. [47] where the meso-SDA was added before the phosphoric acid. The amounts added were the same as for Synthesis A however the addition order and stirring periods changed according to Figure 3.2. Al_2O_3 was dissolved in distilled water and TEA was added dropwise and stirred for one hour. Then SiO_2 was added and the solution was stirred for two hours. The meso-SDA was added dropwise to the gel solution and stirred for 30 minutes before H_3PO_4 was added and stirred for an additional 30 minutes. The gel solution was crystallized, washed and dried with the same parameters as Synthesis A. This synthesis was named **Synthesis B** as the meso-SDA was added **before** the ortho-phosphoric acid, and the samples were marked with the letter **b** at the start of the sample name.
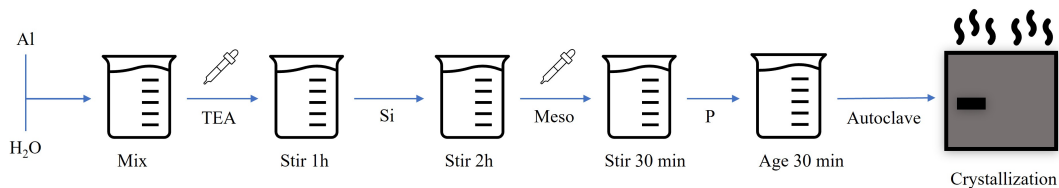
Figure 3.2: Schematic illustration of Synthesis B inspired by Mariatti et. al.[47]

3.3.2 Experiment investigating crystallisation time

The effect of crystallisation time on the synthesis of hierarchical SAPO-5 was investigated in an experiment using Synthesis B. For this experiment, the crystallisation time varied from 48 to 96 hours for glucose and 48 to 144 hours for sucrose, while the molar ratio of meso-SDA added was kept constant at 0.025 and the crystallisation temperature was lowered to 150°C for all samples. The samples were labelled according to their parameters with crystallisation time in parenthesis as bG0.025(72).

3.3.3   Experiment investigating crystallisation temperature

A temperature trial was conducted to find the temperature of glucose and sucrose decomposition during the crystallisation conditions used for these experiments. An aqueous solution of sucrose and glucose was made with a 0.05 molar ratio of meso-SDA/Al and 37.8 g of distilled water to imitate the same conditions for synthesis. The solutions were heated at 125 and 100 °C for 24 hours.

The results from this temperature study suggested that a different crystallisation temperature should be tested. Inspired by literature [61], a different crystallisation procedure was investigated with Synthesis B. A new silicon source was utilized for this experiment as the previous one was empty, where the new precursor had a weight percentage of 30% instead of the previously used 40%. This change in wt.% was discovered after the experiment was conducted, and the samples therefore exhibited a new theoretical molar ratio of precursor shown in Equation 3.3. Other than the new silicon ratio, the rest of the Synthesis followed Synthesis B.

$$1.00\ \text{Al} : 1.00\ \text{P} : 0.15\ \text{Si} : 0.60\ \text{TEA} : X\ \text{Meso-SDA} : 30.00\ \text{H}_2\text{O} \qquad (3.3)$$

The gel solutions were transferred into the stainless steel Teflon lined autoclave and heated in the oven for 24 hours at 90°C, before the samples were crystallised at higher temperatures for 120 hours. The crystallisation temperatures used were 150 and 200°C, and the meso-SDA used was sucrose. The amount of sucrose added had a 0.05 and 0.025 molar ratio. A sample from this experiment was named bS0.05(24/120)-90/200 to represent the pre-crystallisation step, however for simplicity, the same sample was often referred to as bS0.05-90/200.

3.4   Overview all samples

An overview of all experiments and samples and the parameters varied within each experiment is shown in Table 3.1. The naming of each sample reflected what parameters were varied, where a and b at the beginning of the name refer to the synthesis addition order, the G or S refer to the type of meso-SDA followed by the molar ratio of meso-SDA used, then crystallisation time was given in parenthesis followed by crystallisation time at the end of the name. A sample named aG0.05(24)-200 was therefore synthesised with Synthesis **A**, adding 0.05 molar ratio of **G**lucose, and was crystallised for 24 hours at 200°C.

Table 3.1: Overview of samples and synthesis parameters varied for all the samples, showing addition order, meso-SDA to Al ratio, crystallisation time and temperature.

Experiment	Sample name	Addition order	Meso-SDA/Al ratio	Crystallisation time (h)	Crystallisation temp (°C)
Standard	C-SAPO-5	-	-	24	200
Addition order	aG0.025	G **a**fter P	0.025	24	200
	aG0.05	G **a**fter P	0.05	24	200
	aG0.1	G **a**fter P	0.1	24	200
	aG0.2	G **a**fter P	0.2	24	200
	aG0.3	G **a**fter P	0.3	24	200
	aS0.025	S **a**fter P	0.025	24	200
	aS0.05	S **a**fter P	0.05	24	200
	aS0.1	S **a**fter P	0.1	24	200
	bG0.025	G **b**efore P	0.025	24	200
	bG0.05	G **b**efore P	0.05	24	200
	bG0.1	G **b**efore P	0.1	24	200
	bS0.025	S **b**efore P	0.025	24	200
	bS0.05	S **b**efore P	0.05	24	200
	bS0.1	S **b**efore P	0.1	24	200
Crystallisation time	bS0.025(48)	S **b**efore P	0.025	48	150
	bS0.025(72)	S **b**efore P	0.025	72	150
	bS0.025(96)	S **b**efore P	0.025	96	150
	bS0.025(120)	S **b**efore P	0.025	120	150
	bS0.025(144)	S **b**efore P	0.025	144	150
	bG0.025(48)	G **b**efore P	0.025	48	150
	bG0.025(72)	G **b**efore P	0.025	72	150
	bG0.025(96)	G **b**efore P	0.025	96	150
Crystallisation temperature	bS0.025-90/150	S **b**efore P	0.025	24+120	90+150
	bS0.025-90/200	S **b**efore P	0.025	24+120	90+200
	bS0.05-90/150	S **b**efore P	0.05	24+120	90+150
	bS0.05-90/200	S **b**efore P	0.05	24+120	90+200

3.5 Characterisation methods

As stated in the synthesis Section 3.2, the samples were checked for phase purity and then calcined. After calcination, the samples were characterised by a number of different characterisation techniques. This was done to establish whether the hierarchical SAPO-5 was produced successfully and to gain information on the samples' crystallinity, surface and pores, morphology, composition and active sites.

3.5.1 X-ray diffraction

To investigate the phase purity and the crystallinity of the samples, powder XRD was performed with a Bruker D8 A25 DaVinci X-ray Diffractometer with CuKα radiation (1.5046 Å) and a LynxEye$^{\text{TM}}$ SuperSpeed Detector. The analysis was set to crystalline samples with a step size of approximately 0.013°. The program ran for 30 minutes recording the diffractogram from 5-75° and a fixed divergence slit at 0.1° was used for all samples. The diffractograms were baseline corrected when needed and used to establish phase purity in accordance with the AFI framework. They were also used to calculate relative crystallinity with line intensities at 2θ equal to 7.5°, 14.9°, 19.8°, 21.1°, 22.5° and 26.0° using the conventional SAPO-5 sample as a standard for the calculations [12]. The intensities of these six reflections were integrated with Origin software$^{\text{TM}}$ to find the area beneath which was used to calculate crystallinity according to Equation 2.2.

3.5.2 Nitrogen physisorption

To investigate the surface and pores of the material, nitrogen physisorption analysis was performed with a Tristar 3000 Micromeritics Surface Area and Porosimetry Analyser. The samples were degassed in vacuum at 250°C for 18 hours before analysis with a Micromeritics VacPrep$^{\text{TM}}$ 061 to remove water and other adsorbates in the pores. The analysis was done with liquid nitrogen at -196°C, and the SSA was calculated from adsorption isotherms, see theory section 2.5.2, using the BET model. BJH analysis was also performed to calculate the PSD and average pore size of the samples. Mesopore volume was calculated by subtracting the micropore volume from the total single-point adsorption volume.

3.5.3 Inductively coupled plasma - mass spectroscopy

To determine the experimental molar ratio of the samples, ICP-MS was performed with a High Resolution Inductively Coupled Plasma Element 2 and the Agilent - 8800 ICP-MS Triple Quad. The samples were prepared for analysis by digesting

around 20-50 mg of the sample in a solution of concentrated hydrofluoric acid (HF, 40%, 0.5 g) and concentrated nitric acid (HNO$_3$, 65%, 1.5 mL). The solution was left to digest until all of the samples were fully decomposed before the solution was diluted with mili-Q water to a concentration of 0.05 M HF and 0.1 M HNO$_3$. In order to clear any background noise in the analysis, blanks were prepared with the same procedure, without any samples.

3.5.4 Scanning electron microscopy

Scanning electron microscopy was performed to determine particle size and morphology with a Hitachi S-3400N. A small amount of the sample was scattered onto a carbon tape that was attached to the sample holder, and any excess sample was removed. The sample holder was mounted to the instrument, and pictures were captured in secondary electron mode with magnifications of 8 × 270, 850 and 2500 SE. The average particle diameter was calculated using the ImageJ$^{\text{TM}}$ software.

3.5.5 Fourier-transform infrared spectroscopy

Fourier-transform Infrared Spectroscopy was performed with a Bruker Vertex 80 spectrometer using a Liquid Nitrogen cooled Mercury Cadmium Telluride (LN-MCT) detector from Kolmar Technologies to evaluate the relative amount of acid sites in the samples. The detector was cooled to −196°C, and background measurements were taken with a resolution of 1 cm^{-4} with the detector set to an aperture setting of 4 mm and a scanner velocity of 20 kHz. A small amount of sample was pressed into a thin wafer of around 5-15 mg, which was placed in a Specac GS05850 High Temperature High Pressure (HTHP) transmission cell. The sample was heated to 500°C at 5°C/min while a spectrum was measured every minute, and then kept at this temperature for one hour to remove any adsorbed water. After the dehydration, the sample was stepwise cooled to 450°C, 400°C, 300°C, 200°C and 100°C, measuring the spectrum at each step.

The spectra were normalised by dividing with the sample weight and were used to find the relative amount of acid sites in each sample using the conventional SAPO-5 as a standard. The peaks were identified with help of literature [15], and the area beneath was integrated. The areas were then used to calculate a relative amount of acid sites.

4 Results

When collecting results from the characterisation of the samples, it was important to establish what indicated a "good" sample in relation to the project and the research question. An initial list of requirements was therefore made to establish what samples could undergo further characterisation. These included results from the X-ray diffraction and the nitrogen physisorption techniques.

As the goal of this thesis was to synthesise a hierarchical SAPO-5 suitable for catalysis, it was important to have a phase pure sample. Therefore samples with relative crystallinity above 70% and little to no impurities were deemed the first requirement for a good sample. Furthermore, as the high surface area of the material is an important factor for its catalytic abilities, the BET surface area should be above or close to the minimum range found in literature for SAPO-5 materials at 204 m²/g [54]. Lastly, as the material should be considered hierarchical, it was important that the sample has high volumes of both micropores and mesopores, and displays a PSD with defined mesopore width.

4.1 Synthesis of conventional SAPO-5

The diffractograms from XRD analysis of the conventional microporous SAPO-5 are shown in Figure 4.1.
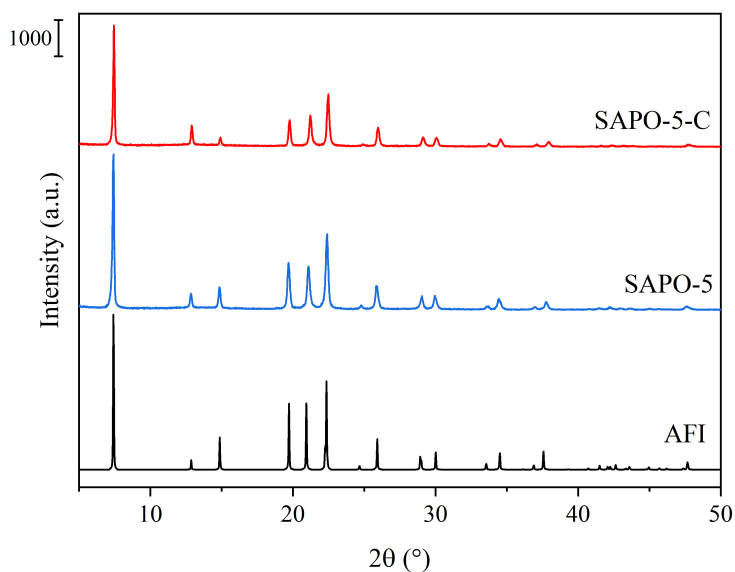

Figure 4.1: Diffractograms of conventional SAPO-5 before (SAPO-5) and after (SAPO-5-C) calcination, compared with the AFI framework [13].

As the figure shows, there was no structural collapse after calcination (SAPO-5C) and as the sample exhibited good phase purity when compared to the AFI framework, it was deemed good for use as a standard. There can be observed a clear change in the intensity of the reflections at around 12.2° and 14.9° which is a common observation when SAPO-5 is calcined [62]. The powder of the conventional microporous SAPO-5 after it was washed and dried was white as shown in Figure 4.2.A. The colour maintained white after calcination as shown in Figure 4.2.B.
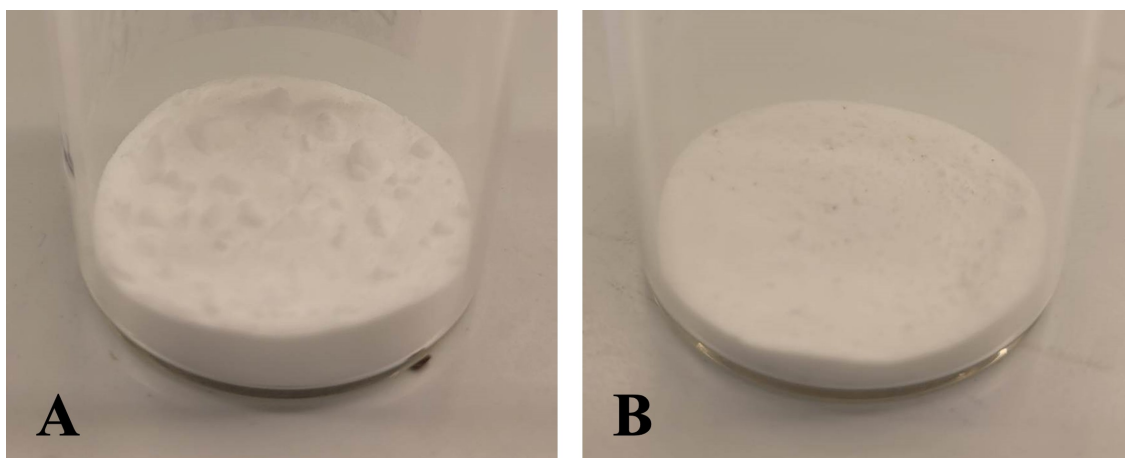
Figure 4.2: Images taken of the powder samples before A and after B calcination of the standard C-SAPO-5 sample.

4.2   Observations from hierarchical synthesis

During the synthesis of hierarchical samples, all samples came out of the autoclaves after crystallisation looking brown, see Figure 4.3. This was not the case after the crystallisation of the conventional microporous SAPO-5, which appeared as a clear yellow solution. As the meso-SDA was the only new element for Synthesis A, it seemed reasonable to assume that the brown colouring came from the decomposition of glucose and sucrose.

The as-prepared samples still exhibited a brown colouring after washing and drying, as shown on the right in Figure 4.3 for sample aG0.1. It was difficult to remove all the organic material in the water during washing and some organic waste was dried along the sample, shown in the figure as the black spots in the dish.
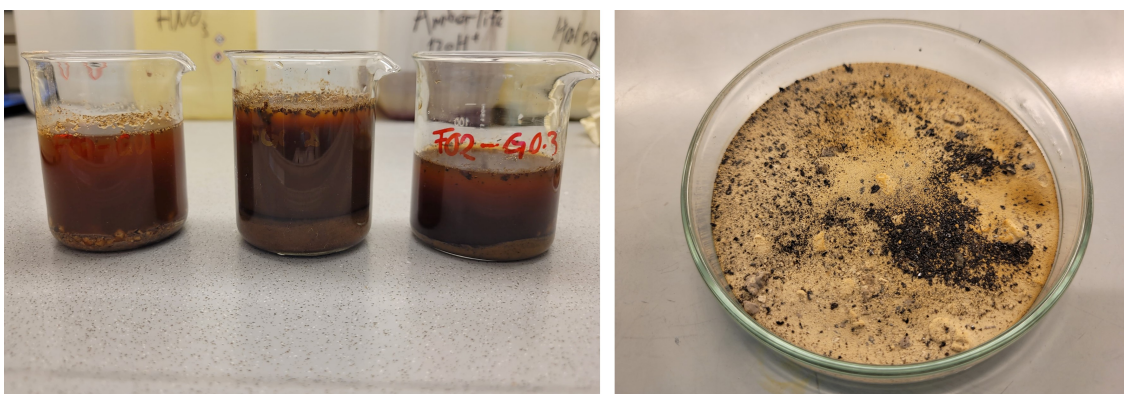
Figure 4.3: Images taken during Synthesis A of sample aG0.1, aG0.2 and aG0.3, on the left taken after crystallisation and before washing, and on right showing sample aG0.1 after drying for 72 hours at 70°C.

However, after the as-prepared samples were calcined, most of the brown colouring seemed to be removed for samples with Synthesis A, suggesting that all the organic material was combusted during calcination. This can be observed in Figure 4.4 where samples from Synthesis A are displayed before calcination at the top and after calcination at the bottom.

Figure 4.4: Images taken of the powder samples before (A) and after (B) calcination of the samples with synthesis A from experiment investigating addition order.

This whitening of the sample after calcination was not observed for the samples with Synthesis B, shown in Figure 4.5. In this synthesis, as-prepared samples appeared

significantly darker in colour compared with Synthesis A, and after calcination samples appeared in various shades of grey. Because samples did not appear white after calcination, it suggested that the synthesis addition order produced a powder with an organic phase that was difficult to remove. It could also suggest that the samples contained other phases than the white SAPO-5, however this had to be investigated with further characterisation.
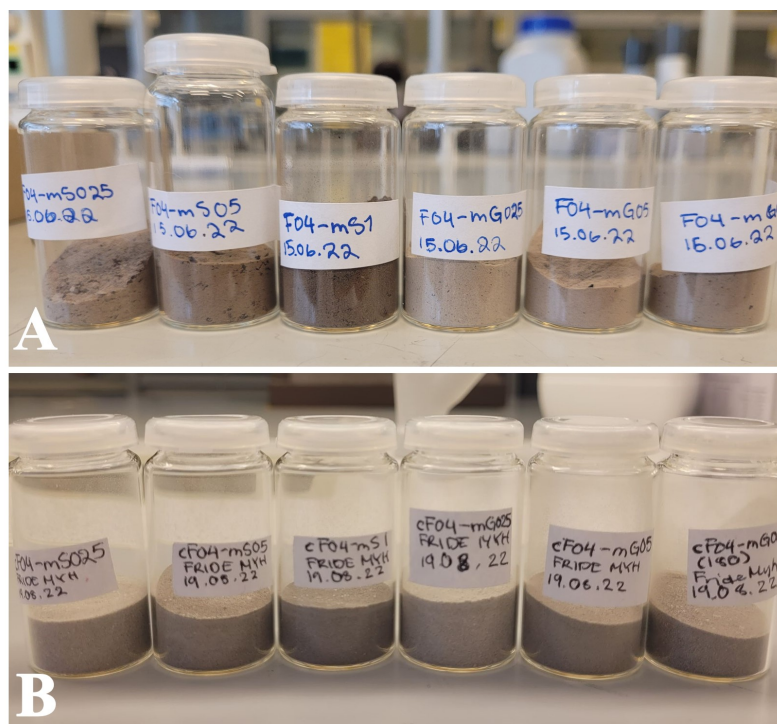
Figure 4.5: Images taken of the powder samples before (A) and after (B) calcination of the samples with synthesis A from experiment investigating addition order.

Other observations were also obtained from the appearance of the powders. First of all, it seemed that the colour depended on the type of meso-SDA used in synthesis. The sucrose samples were a darker brown both for Synthesis A and B, compared to the glucose samples, which can be clearly seen with the as-prepared samples in Figure 4.5 where the three first samples are sucrose, and the three latter are glucose. This was also observed after calcination where the sucrose samples in Synthesis A displayed a yellow-white colouring, while the glucose samples appeared more white, see Figure 4.4 where the three first are sucrose and the next two are glucose. For Synthesis B, the grey colouring after calcination was darkest for the sucrose samples.

Secondly, when looking at the varying meso-SDA/Al ratio used in synthesis, it seemed like the increased ratio resulted in a darker colour for the as-prepared samples. This was observed for both syntheses, where the 0.025 ratio appeared the

lightest, and the highest ratio appeared the darkest. This seemed to confirm the hypothesis that the colouring derived from the combusted glucose and sucrose. While the discolouration disappeared after calcination for synthesis A, it persisted for synthesis B.

4.3   Results from X-ray diffraction

In the following chapter, results from the XRD analysis of the hierarchical samples are presented and any trends or observations are elucidated. The diffractograms presented in the figures are the calcined samples, whereas the diffractograms from the as-prepared samples can be found in Appendix A. The results will be presented in order of what parameter was investigated with the samples.

4.3.1   Experiment investigating addition order

Mainly the addition order of the precursors and template was varied in the first experiment. Multiple samples were synthesized using the two synthesis methods with both meso-SDAs as well as with varying meso-SDA/Al ratio. The diffractograms of Synthesis A, where meso-SDA was added after the phosphoric acid, are displayed in Figure 4.6, with glucose on the left and sucrose on the right. It appeared that Synthesis A produced phase pure samples for both meso-SDAs and for all ratios added to the synthesis gel.
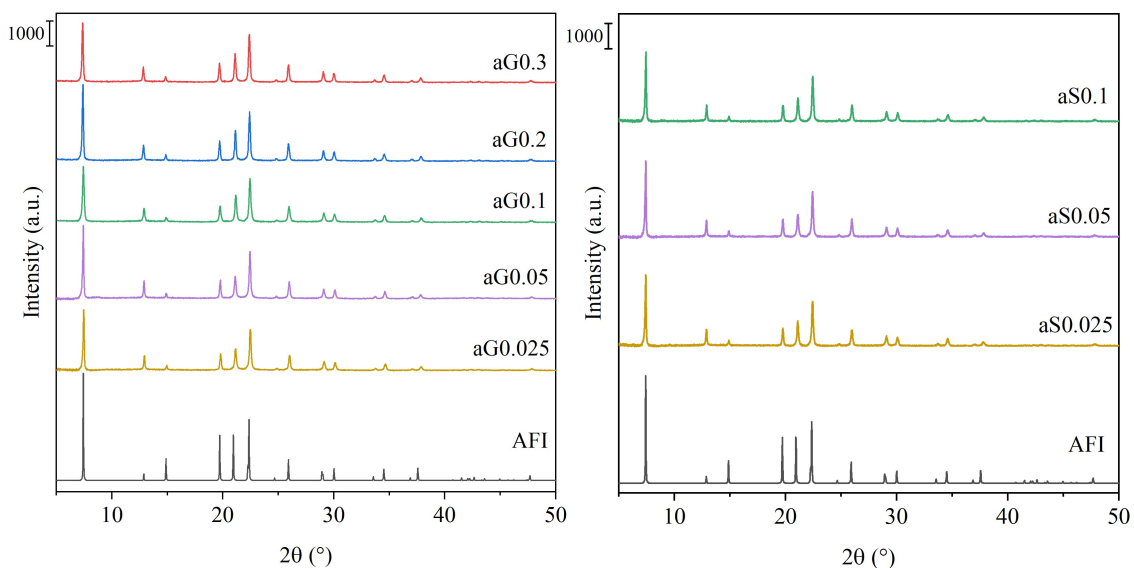

Figure 4.6: Diffractograms of calcined samples from Synthesis A with varying meso-SDA ratio from 0.025-0.3 for glucose on the left and from 0.025-0.1 for sucrose on the right. All samples were crystallised at 200°c for 24 hours.

The diffractograms displayed no clear trends in relation to meso-SDA/Al ratio, nor any significant differences in relative crystallinity between glucose and sucrose, given in Table 4.1. The calculated relative crystallinities were all approximately 100%, suggesting that Synthesis A was successful in producing phase pure SAPO-5 materials, deeming all samples from Synthesis A suitable for nitrogen physisorption analysis.

Table 4.1: Relative crystallinity for experiment investigating addition order calculated from Eq. 2.2 using conventional SAPO-5 as a standard, whether the samples are considered phase pure (pure Tridymite samples are marked not applicable) and the dominating phase present.

Sample name	Relative crystallinity (%)	Phase pure?	Dominating phase
C-SAPO-5	100	✓	AFI
aG0.025(24)-200	100	✓	AFI
aG0.05(24)-200	99	✓	AFI
aG0.1(24)-200	98	✓	AFI
aG0.2(24)-200	109	✓	AFI
aG0.3(24)-200	94	✓	AFI
aS0.025(24)-200	108	✓	AFI
aS0.05(24)-200	106	✓	AFI
aS0.1(24)-200	100	✓	AFI
bG0.025(24)-200	63		AFI
bG0.05(24)-200	27		Tridymite
bG0.1(24)-200	4		Tridymite
bS0.025(24)-200	52		AFI
bS0.05(24)-200	44		AFI
bS0.1(24)-200	N/A		Tridymite

The diffractograms from the samples produced with Synthesis B, where meso-SDA was added before the phosphoric acid, are given in Figure 4.7. The overall observation was that all samples showed some degree of impurities of another phase identified as Tridymite. The reflections of the impurities were located at around 20.3, 21.5 and 22.9 2θ, marked with an asterisk on the figure, where Tridymite dense phase have similar reflections in literature [12, 16, 63]. Tridymite is a common byproduct to AFI materials [11, 12] and for sample bG0.1(24)-200 and bS0.1(24)-

200, it was the dominating phase where little to no AFI reflections were present. For both glucose and sucrose, it seemed like the Tridymite phase increased with an increasing amount of meso-SDA added. It can be observed when looking at the first AFI reflection at around 7.4°2θ that the reflection has the highest intensity at 0.025 meso-SDA ratio and is absent at 0.1 meso-SDA ratio. This can also be noted for the crystallinities given in Table 4.1, where the 0.025 ratio samples gave the highest relative crystallinity of 63% for glucose and 52% for sucrose and lowest for the 0.1 ratio with 4% for glucose and N/A for sucrose.
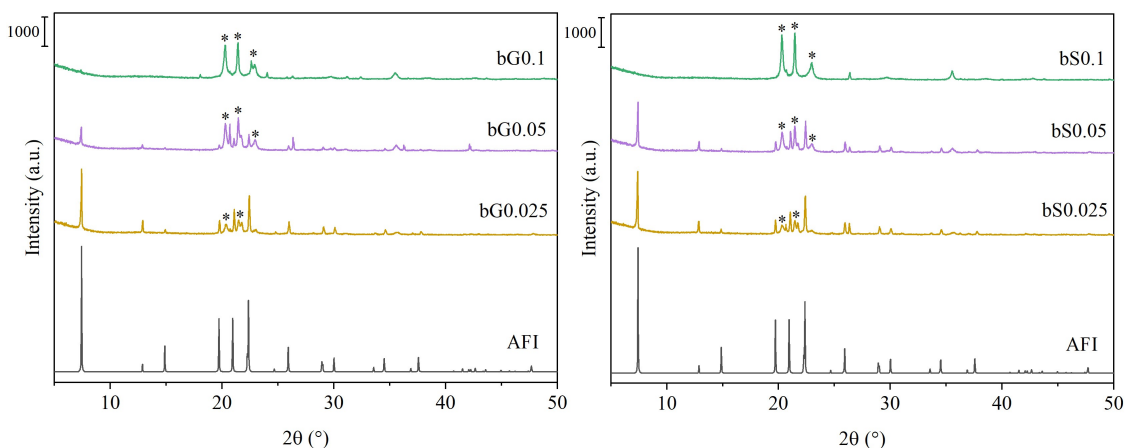
Figure 4.7: Diffractograms of the samples from synthesis B with varying meso-SDA ratio from 0.025-0.1 for Glucose on the left and for sucrose on the right. All samples were crystallised at 200°C for 24 hours. The asterisks mark the reflections for the Tridymite phase.

Finally, when comparing the type of meso-SDA, glucose gave a higher relative crystallinity for the 0.025 at 63% ratio than sucrose at 52%, and the amount of Tridymite phase seemed to be equal for the two samples. However, for the 0.05 samples, sucrose gave a significantly higher relative crystallinity than glucose, with 44% versus 27% for glucose.

In summary, while Synthesis A resulted in phase pure and highly crystalline samples, Synthesis B resulted in the presence of a Tridymite phase in all samples as well as a low crystallinity. For Synthesis B, samples with the lowest meso-SDA ratio of 0.025 displayed the highest relative crystallinities and the least amount of Tridymite phase. Therefore, it seemed reasonable to further attempt to adjust Synthesis B with this ratio to eliminate the Tridymite impurities and achieve a higher crystallinity. This was attempted by increasing the crystallisation time.

4.3.2 Experiment investigating crystallisation time

This experiment was conducted to investigate the effect of increasing the crystallisation time for Synthesis B, with a meso-SDA ratio of 0.025 and a crystallisation temperature of 150°C as an attempt to avoid the decomposition of the meso-SDA as glucose is known to decompose at 188°C [64]. The experiment started with three samples for both glucose and sucrose, varying the crystallisation time from 48 hours to 96, however was continued with two new samples of 120 and 144 hours for sucrose. The diffractograms for the samples produced in the experiment investigating crystallisation time are shown in Figure 4.8.
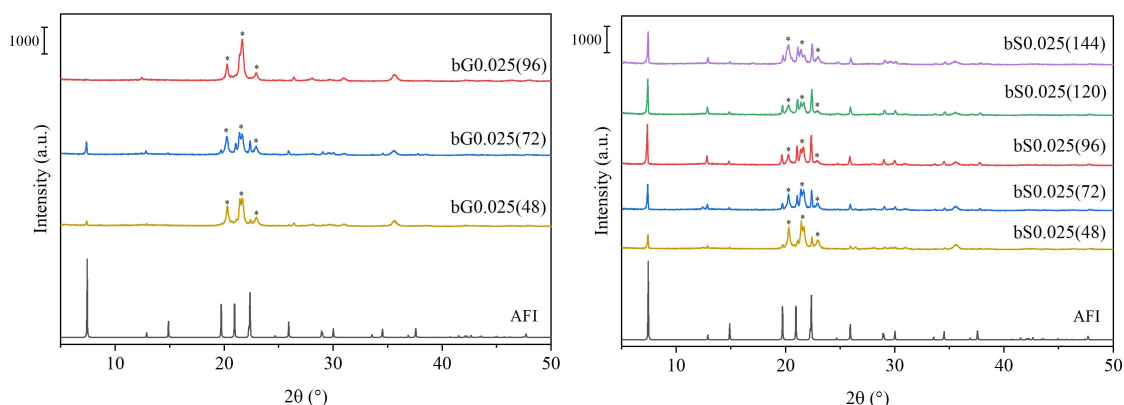
Figure 4.8: XRD diffractograms of samples from experiment varying crystallisation time, on left samples with glucose and on right sucrose. All samples were crystallised at 150°C. The asterisks mark the reflections for the Tridymite phase.

The diffractograms of the glucose show a slight increase in intensity from 48 to 72 hours, and relative crystallinity increases from 12% at 48 hours to 25% for 72 hours, see Table 4.2. The Tridymite intensities seemed to decrease from the 0.025 to the 0.05 ratio, however at 96 hours, the diffractogram was completely dominated by the Tridymite phase. This concludes that for glucose, 72 hours was the optimal crystallisation time, although the relative crystallinity was significantly lower than the bG0.025-200 sample from the previous at 63%, suggesting that the lowered temperature produced less phase pure samples.

32

Table 4.2: Relative crystallinity for experiment investigating crystallisation time calculated from Eq. 2.2 using conventional SAPO-5 as a standard, whether the samples are considered phase pure (pure Tridymite samples are marked not applicable) and the dominating phase present.

Sample name	Relative crystallinity (%)	Phase pure?	Dominating phase
C-SAPO-5	100	✓	AFI
bS0.025(48)-150	22	×	Tridymite
bS0.025(72)-150	31	×	Tridymite
bS0.025(96)-150	47	×	AFI
bS0.025(120)-150	44	×	AFI
bS0.025(144)-150	37	×	Tridymite
bG0.025(48)-150	12	×	Tridymite
bG0.025(72)-150	25	×	Tridymite
bG0.025(96)-150	N/A	×	Tridymite

The intensity of the Tridymite reflections on the sucrose samples seemed to display a trend where the phase decreases with increasing crystallisation time. When looking at the first Tridymite reflection marked with an asterisk in Figure 4.9, it is clear that the Tridymite phase decreases from 48 to 120 hours. However at 144 hours, the intensity increases again. This suggests that a longer crystallisation time promotes less Tridymite phase in the structure, however has an optimal crystallisation time of 120, where the Tridymite phase increases at longer times.
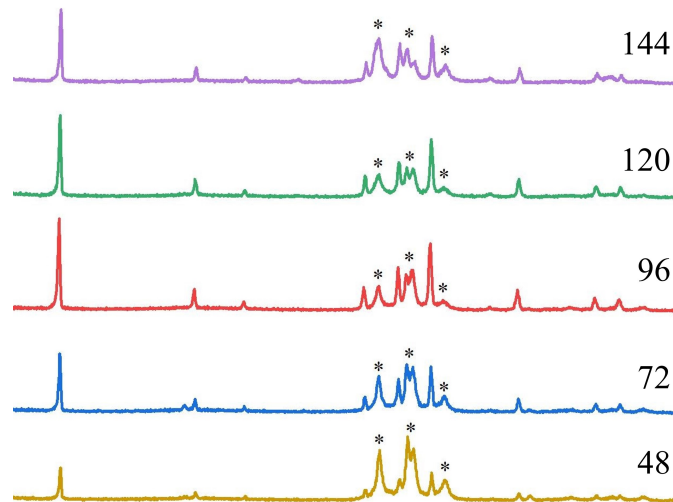

Figure 4.9: Enhanced figure of the changes in intensities in the diffractograms when crystallisation time varies for sucrose, on bottom sample bS0.025(48) and on top bS0.025(144).

When looking at the AFI crystallinity calculated, 96 hours seem to be optimal as this sample gave the highest crystallinity of 47%, see Table 4.2. In Figure 4.10, the crystallinities of the five sucrose samples are plotted together suggesting 96 hours to be the optimal crystallisation time for the AFI phase.
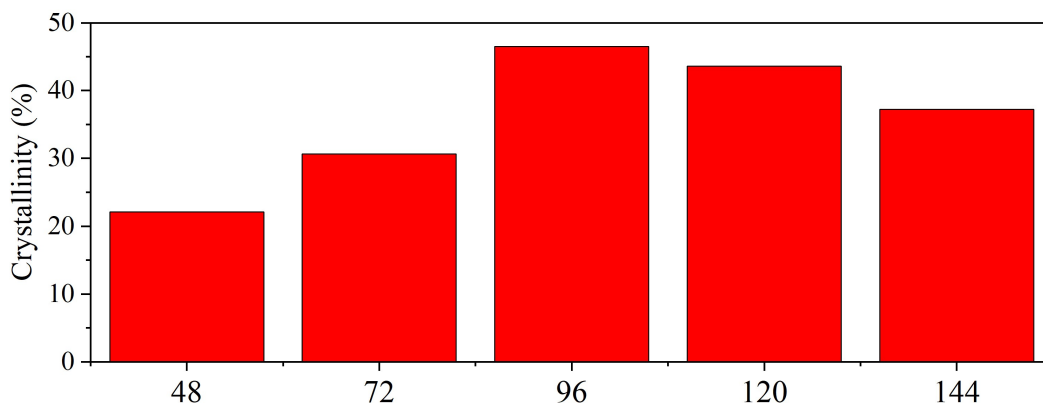
Figure 4.10: Relative crystallinities of the sucrose diffractograms from experiment investigating crystallisation time, all samples crystallised at 150°C.

In summary for this experiment, both glucose and sucrose seem to reach an optimum crystallisation time for the AFI phase at 72 and 96 hours respectively, and an optimum time for removing the Tridymite phase for sucrose at 120 hours. However no samples gave a relative crystallinity above Synthesis B samples from the previous experiment suggesting that lowering the crystallisation temperature to 150°C, reduced the crystallinity.

4.3.3   Experiment investigating crystallisation temperature

Despite lowering the crystallisation temperature in the previous experiment to 150°C, samples still came out from crystallisation looking brown as the samples from synthesis A in Figure 4.3, suggesting that the meso-SDA decomposed during crystallisation. As mentioned in the theory section however, hydrothermal synthesis occurs under supercritical conditions, which may affect the temperature of decomposition of the meso-SDAs. Two temperature trials were therefore conducted in autoclaves, where the results are shown in Figure 4.11. The results suggested that when heating the sucrose (A) and glucose (B) solutions at 100°C, no decomposition occurred. However at 120°C, both sucrose (C) and glucose (D) solutions displayed a dark brown colour suggesting that the point of decomposition was somewhere between these two temperatures.
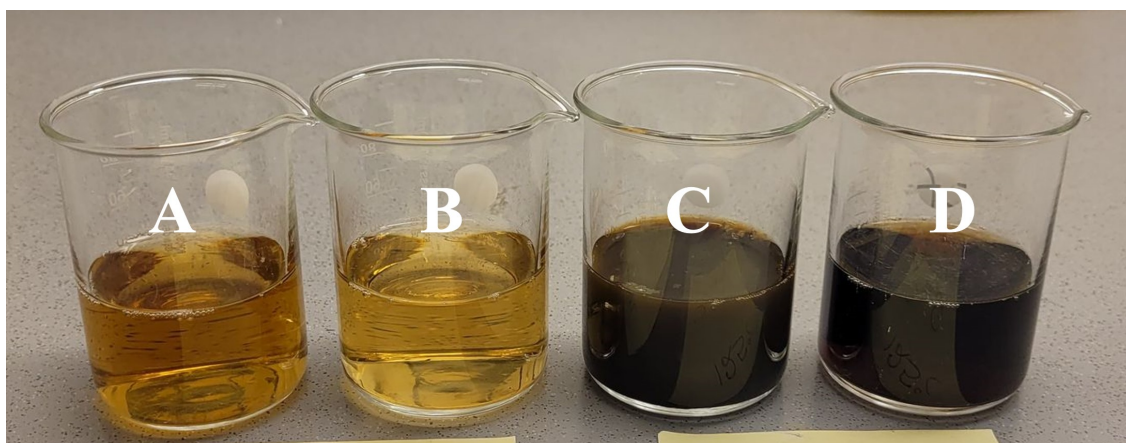
Figure 4.11: Image of results from temperature trial, showing sucrose solutions (A and C) and
glucose solutions (B and D) where A and B was heated in an autoclave at 100°C
and C and D at 125°C.

It should however be noted that synthesising SAPO-5 has been reported to only
be possible above a temperature of 150°C, where using lower crystallisation tem-
peratures promotes the formation of other crystalline phases in the structure [11].
A low-temperature pre-crystallisation step was there added to investigate if this
would affect the crystallinity. The diffractograms from this experiment are shown
in Figure 4.12, where sucrose was used for all samples as this showed more promise
from the previous experiment.
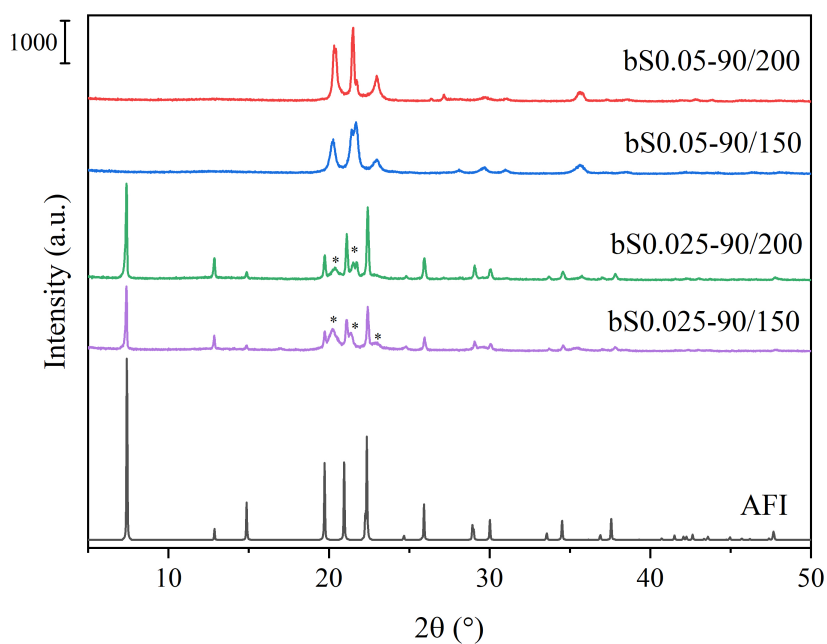
Figure 4.12: XRD diffractograms of samples that were heated to 90°C for 24 hours before crys-
tallisation for 120 hours at 150 or 200°C.

The samples using a 0.05 sucrose ratio, red and blue diffractograms, for crystallisation temperatures of 200 and 150°C respectively, displayed a pure Tridymite phase with no AFI phase present. The green and purple diffractogram referring to the samples with 0.025 sucrose ratio, displayed the AFI framework with relative crystallinities of 75% and 49% for 200 and 150°C respectively, see Table 4.3. It seemed like the higher crystallisation temperature increased the crystallinity and decreased intensities for the Tridymite phase.

Table 4.3: Relative crystallinity for experiment investigating crystallisation temperature calculated from Eq. 2.2 using conventional SAPO-5 as a standard, whether the samples are considered phase pure (pure Tridymite samples are marked not applicable) and the dominating phase present.

Sample name	Relative crystallinity (%)	Phase pure?	Dominating phase
C-SAPO-5	100	✓	AFI
bS0.025(24/120)-90/150	49	×	AFI
bS0.025(24/120)-90/200	75	✓	AFI
bS0.05(24/120)-90/150	N/A	×	Tridymite
bS0.05(24/120)-90/200	N/A	×	Tridymite

In summary, the Tridymite reflections were significantly lower in intensity for sample bS0.025-90/200 compared to the samples from the previous experiment with Synthesis B, suggesting that the pre-crystallisation step under those parameters promoted the production of the AFI phase and demoted Tridymite. With a relative crystallinity above 70% and with relatively low Tridymite impurities, sample bS0.025(24/120)-90/200 was included in samples to move forward with from XRD analysis.

4.4   Samples chosen for nitrogen physisorption

As previously mentioned, the samples chosen for nitrogen physisorption were samples with relative crystallinity higher that 70% and with little to no impurities. Sample bG0.025(24)-200 from the experiment investigating addition order was also included in the analysis, because at the time, it showed the most promise from Synthesis B, and with a relative crystallinity of 63% seemed good enough for comparison within the experiment. An overview of the samples chosen for further analysis is given in Table 4.4 showing relative crystallinity and phases present.

Table 4.4: Summery of samples with a crystallinity > 70% from XRD analysis showing relative crystallinity and phases present in diffractograms.

Synthesis	Sample name	Relative Crystallinity (%)	Phases present
Standard	C-SAPO-5	100	AFI
A	aG0.025(24)-200	100	AFI
	aG0.05(24)-200	99	AFI
	aG0.1(24)-200	98	AFI
	aG0.2(24)-200	109	AFI
	aG0.3(24)-200	94	AFI
	aS0.025(24)-200	108	AFI
	aS0.05(24)-200	106	AFI
	aS0.1(24)-200	100	AFI
B	bG0.025(24)-200	63	AFI + Tridymite
	bS0.025(24/120)-90/200	75	AFI + Tridymite

4.5   Results from nitrogen physisorption

In this chapter, results from the nitrogen physisorption analysis are presented for the samples chosen from XRD. The BET and BJH methods were used to investigate the surface area, pore volumes, pore size distributions and adsorption isotherms, with results presented in the same order. An overview of results from the analysis is given in Table 4.5, giving BET, micropore and external surface area and total, micropore and mesopore volume for each sample.

Table 4.5: Data from N_2 physisorption analysis, showing BET surface area, t-plot micropore and external surface area, singe point adsorption total volume, t-plot microporous volume, calculated mesoporous volume and BJH adsorption average pore width.

Sample name	Surface area (m^2/g)			Pore volume (cm^3/g)		
	BET	**Micro**	**Ext**	**Total**	**Micro**	**Meso**
C-SAPO-5	218	161	58	0.12	0.08	0.04
aG0.025(24)-200	271	202	68	0.16	0.10	0.05
aG0.05(24)-200	183	122	60	0.11	0.06	0.05
aG0.1(24)-200	293	241	51	0.17	0.12	0.04
aG0.2(24)-200	305	247	59	0.18	0.13	0.06
aG0.3(24)-200	338	270	68	0.20	0.14	0.06
aS0.025(24)-200	248	200	48	0.14	0.10	0.03
aS0.05(24)-200	268	214	54	0.15	0.11	0.04
aS0.1(24)-200	246	198	49	0.15	0.10	0.05
bG0.025(24)-200	147	102	44	0.18	0.05	0.13
bS0.025(24/120)-90/200	178	133	45	0.15	0.07	0.08

4.5.1   Surface areas and pore volumes

Looking at the BET surface area values in Table 4.5, the standard C-SAPO-5 among most other samples exhibit a BET surface area above the minimum value found in literature [54] at 204 m^2/g. The exception are two samples from Synthesis B, bG0.025(24)-200 and bS0.025(24/120)-90/200 and sample aG0.05(24)-200 from Synthesis A.

Comparing the hierarchical samples with the standard, it is observed that all samples from Synthesis A have a higher BET surface area than the standard, except aG0.025 and the two samples from Synthesis B have a significantly lower BET area than the standard. As both Synthesis B samples exhibited impurities in the diffractograms from XRD, it can suggest that the Tridymite phase decreased the surface

area. On the other hand, sample aG0.025 exhibited a phase pure diffractogram, and also had a low BET surface area of 183 m^2/g. It is therefore not conclusive that the lower surface area of synthesis B samples was caused by the Tridymite phase. It is more reasonable to assume that the difference in BET surface area is due to the synthesis addition order, where Synthesis A generally produced samples with higher surface areas compared to synthesis B.

Looking at the samples from Synthesis A with glucose, there seems to be a trend where BET surface area increases with increasing glucose ratio, from 271 - 338 m^2/g. This trend in surface area is shown only for micropore area in the samples which increases from 202 - 270 m^2/g, and not for the external surface area which is fairly constant throughout the samples. Nevertheless, this trend is not observed for samples with sucrose, where BET surface area is highest for the middle meso-SDA ratio.

SAPO-5 have been reported in literature to exhibit a micropore volume of 0.09-0.13 cm^3/g [7, 12, 65]. Hierarchical SAPO-5 samples should exhibit a mesopore volume equal to or higher than the micropore volume to be considered hierarchical [7, 21, 66]. Only hierarchical samples from Synthesis A displayed a micropore volume higher than the minimum literature value at 0.9 cm^3/g, again with the exception of sample aG0.05. The standard C-SAPO-5 sample exhibited a micropore volume of 0.08 cm^3/g, deeming it good enough for comparison as the value is relatively close to literature.

The mesopore volume does increase with increased sucrose ratio for the samples with synthesis A, from 0.03-0.05 cm^3/g, however these values are relatively low. In fact, all samples with Synthesis A exhibited a relatively low mesopore volume close to the mesopore volume of the microporous C-SAPO-5 and would be considered microporous samples when compared to literature. This suggests that the addition order in Synthesis A was not successful in incorporating mesopores in the material, suggesting that the meso-SDA used in synthesis did not work as a template for mesopores.

Synthesis B produced significantly more mesopores than Synthesis A. Sample bG0.025 from the experiment investigating addition order displayed a significantly high mesopore volume of 0.13 cm^3/g. However, the micropore volume for this sample was 0.05, notably lower than the minimum value from literature. Sample bS0.025(24/120)-90/200 from the experiment investigating crystallisation temperature had the same observations as bG0.025(24)-200, however overall presented better results. The micropore volume is lower than literature values, however not as significant with a

volume of 0.07 cm^3/g. In fact, with a mesopore volume of 0.08 cm^3/g, this sample displayed the best micro/meso volume ratio close to what is expected for hierarchical samples.

In summary, it seems that Synthesis B was successful in producing mesopores in the material, however this was at the expense of the micropores, while Synthesis A produced more micropore volume with low values for mesopores.

4.5.2   Physisorption isotherms

The physisorption isotherms of the samples with Synthesis A and sample C-SAPO-5 are shown in Figure 4.13. The isotherm for the standard microporous C-SAPO-5, exhibits a type I isotherm typical for microporous materials, exhibiting a plateau where adsorption levels out, and with no hysteresis loop suggesting the absence of mesopores in the material. The shape resembles the I(a) isotherm suggesting the material exhibits narrow micropores [51].

The shape of all hierarchical samples with Synthesis A exhibits a mixture between type I and IV(a), all samples exhibiting some degree of hysteresis loop. The hysteresis loops closely resemble the H4 defined by De Gruyter [51], and represents mesoporous zeolites, however also exhibit a mesopore structure that is not well-defined.

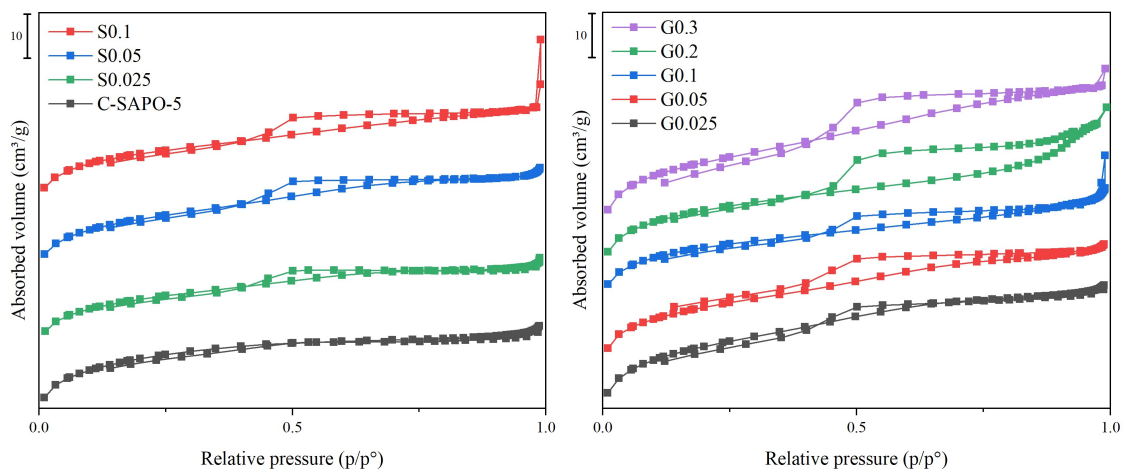**Figure 4.13:** Physisorption isotherms plotting relative pressure against the adsorbed volume of gas, showing the standard C-SAPO-5 sample on the left and samples with synthesis A addition order, with sucrose on the left and sucrose on the right.

The hysteresis loops exhibit various broadness of adsorbed volume, where the sucrose shows a trend where hysteresis broadness increases with increasing sucrose

ratio as sample aS0.025 has the thinnest hysteresis and aS0.1 has the broadest. The broadness of the hysteresis could indicate more mesopore volume, which is in correlation to the values of mesopore volume from the previous chapter, where mesopore volume increased with an increasing sucrose ratio.

No trend is observed with the glucose samples however they also exhibit a variation in hysteresis thickness, where the thickness does correspond to the mesopore volumes previously reported. Sample aG0.3 and aG0.2 have the broadest hysteresis and the highest mesopore volume of 0.06 cm^3/g, sample aG0.1 has a thinner hysteresis and the lowest mesopore volume of 0.04 cm^3/g and sample aG0.5 lies in between for both. Interestingly, sample aG0.025 exhibits a relatively thin hysteresis loop with a mesopore volume of 0.05 cm^3/g.

The adsorption isotherms of the samples from Synthesis B are shown in Figure 4.14 including the C-SAPO-5 isotherm for reference. It looks like the Synthesis B samples are a mix between type II and IV(a) isotherms where type II is given by nonporous or macroporous materials with no limiting adsorption and IV(a) indicating wider mesopores. The isotherms exhibit hysteresis loops that resemble type H3 representing poorly defined mesopores and typically indicating the presence of macroporosity.
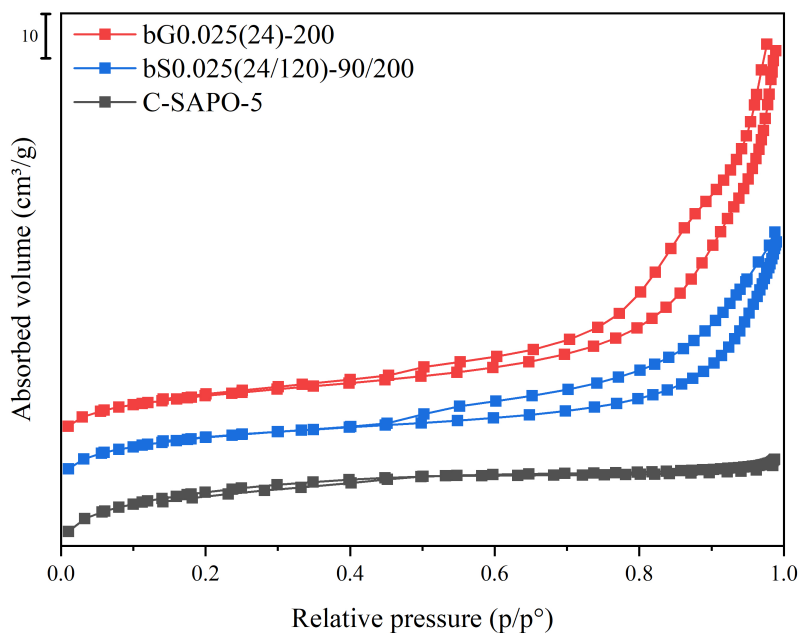

Figure 4.14: Physisorption isotherms plotting relative pressure against the adsorbed volume of gas, showing the two samples with Synthesis B and C-SAPO-5 as a reference.

4.5.3 Pore size distribution

The pore size distribution plots for samples with Synthesis A are shown in Figure 4.15. The distribution curve of C-SAPO-5 is included in both plots as a reference and shows a typical pore size distribution for microporous materials as no prominent features are observed on the distribution curve, indicating little to no mesopores in the structure as the curve fattens.

Some of the glucose samples show distinct shoulders in their distribution curves, especially sample aG0.05 in red, where it looks like two features at 35 and 40 Å. As the isotherm for this sample was not closed, one of the plateaus could relate to the TSE which is usually observed at 38 Å. Samples aG0.025 and aG0.3 also show shoulders in their distribution at around 40 Å, however they are not as defined as the aG0.05 sample suggesting the presence of mesopores. No shoulders were observed for aG0.01 and aG0.2, however the distribution is higher than C-SAPO-5 from around 30 Å, and aG0.2 has a distribution that does not flatten.

No distinct peaks are observed for the sucrose samples from Synthesis A, however all samples exhibit higher pore volumes than C-SAPO-5 in the distribution from around 30-80 Å, which could resemble shoulders. This could suggest that mesopores are present, however with no uniform pore width but rather in a range of sizes.
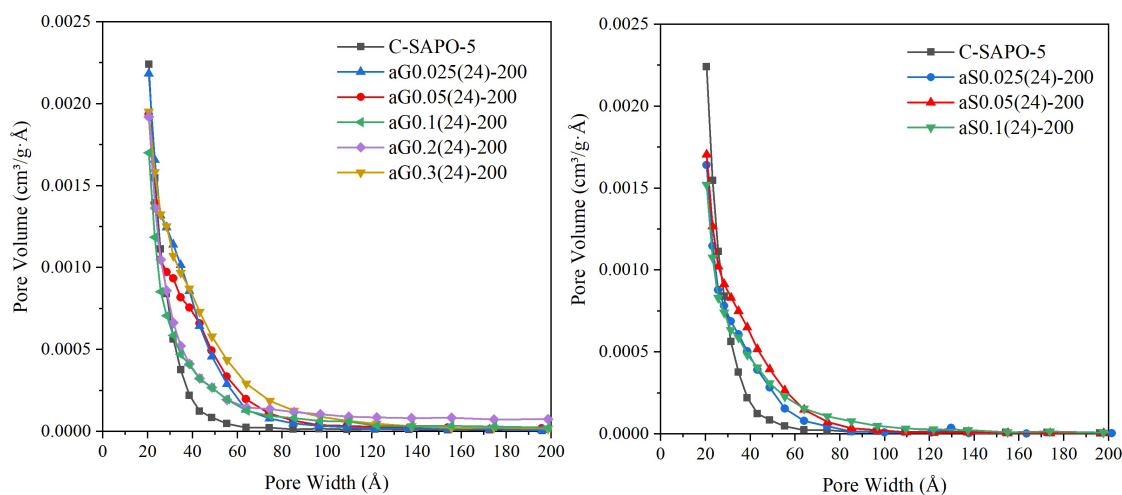
Figure 4.15: BJH pore size distribution plots for samples from Synthesis A and C-SAPO-5 as a reference, with glucose on the left and sucrose on the right.

The distribution curves for the samples with Synthesis B are shown in Figure 4.16, showing no uniform or well-defined pore width. Both samples exhibit an overall higher pore volume than C-SAPO-5 from around 40 Å and higher, suggesting that mesopores are present in these two samples in a wide range of sizes. Sample bG0.025

shows a peak in the distribution at around 125 Å, while sample bS0.025 flattens out at around 50 Å and stays at a higher pore volume than C-SAPO-5.
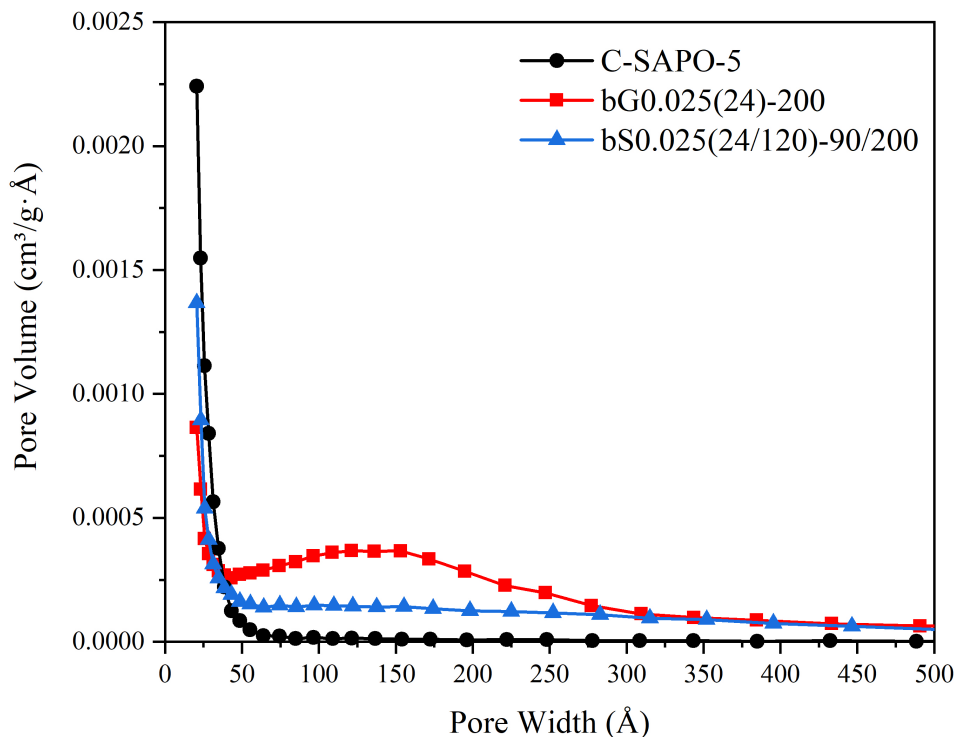
Figure 4.16: BJH pore size distribution plots for samples from Synthesis B and C-SAPO-5 as a reference.

4.6   Inductively coupled plasma - mass spectroscopy

ICP-MS was conducted to investigate the experimental molar ratio of precursors after synthesis, and the effect of the parameters on the composition of the building blocks. The samples chosen for ICP-MS were all the samples from Synthesis A as these were phase pure, displayed high relative crystallinity and had sufficient BET surface area. The bS0.025(24/120)-90/200 sample from the experiment investigating crystallisation temperature was also included as it exhibited good relative crystallinity and would work for comparison as it was the best outcome from Synthesis B. In Table 4.6 the theoretical and experimental molar ratio of the samples are given, and the weight percentages from the analysis are given in Appendix C. The ICP-MS results indicated that most samples had a higher experimental molar ratio of P and a lower ratio of Si compared to the theoretical ratio.

Table 4.6: Data from ICP-MS analysis, the theoretical and experimental molar ratio for each sample analysed.

Sample name	Theoretical molar ratio	Experimental molar ratio
C-SAPO-5	1.00 Al : 1.00 P : 0.20 Si	1.00 Al : 1.05 P : **0.14** Si
aG0.025(24)-200	1.00 Al : 1.00 P : 0.20 Si	1.00 Al : 1.07 P : **0.15** Si
aG0.05(24)-200	1.00 Al : 1.00 P : 0.20 Si	1.00 Al : 1.07 P : **0.16** Si
aG0.1(24)-200	1.00 Al : 1.00 P : 0.20 Si	1.00 Al : 1.02 P : **0.16** Si
aG0.2(24)-200	1.00 Al : 1.00 P : 0.20 Si	1.00 Al : 1.08 P : **0.20** Si
aG0.3(24)-200	1.00 Al : 1.00 P : 0.20 Si	1.00 Al : 1.06 P : **0.12** Si
aS0.025(24)-200	1.00 Al : 1.00 P : 0.20 Si	1.00 Al : 1.03 P : **0.16** Si
aS0.05(24)-200	1.00 Al : 1.00 P : 0.20 Si	1.00 Al : 1.05 P : **0.16** Si
aS0.1(24)-200	1.00 Al : 1.00 P : 0.20 Si	1.00 Al : 1.03 P : **0.18** Si
bS0.025-90/200	1.00 Al : 1.00 P : 0.15 Si	1.00 Al : 1.13 P : **0.13** Si

There were some slight trends to be drawn from the data when looking at the varying meso-SDA ratio for Synthesis A. For glucose, there is a clear trend where the Si/Al ratio increases with increasing meso-SDA ratio, see Figure 4.17. The Si/Al ratio increased from 0.15 to 0.20 from 0.025-0.2 meso-SDA ratio added to the solution gel. However, for the 0.3 meso-SDA ratio, the Si/Al ratio fell drastically to 0.12. This is interesting as the trend would suggest that more glucose promoted more silicon in the structure, however at 0.3, the silicon ratio drops to a level below the conventional SAPO-5.
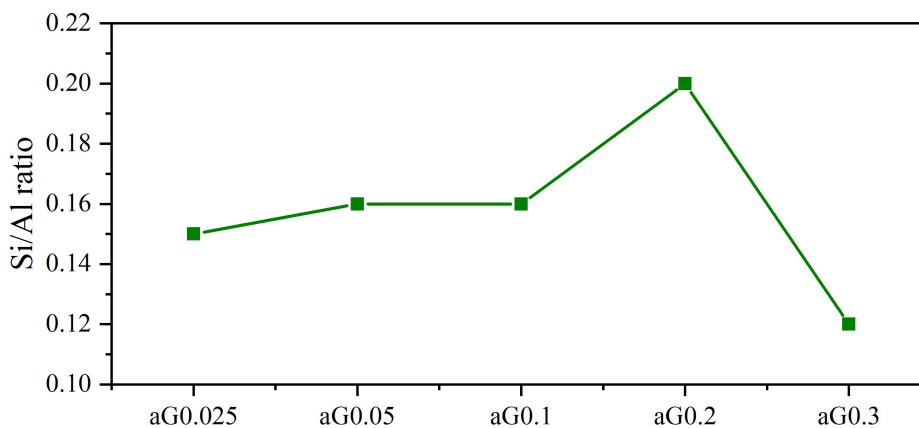
Figure 4.17: Trend showing increase in Si/Al ratio with increased amount of glucose used in synthesis, where Si/Al ratio increases from 0.15-0.20, then drops drastically to 0.12 for sample aG0.3.

4.7   Samples chosen for further analysis

The samples chosen for SEM imaging and FTIR analysis were chosen as the samples most suitable for catalysis. As there have been many parameters studied so was, some consistency was desirable and only samples with a meso-SDA ratio of 0.025 were chosen as the best sample from Synthesis B had this ratio. Sample aG0.025 and aS0.025 from the experiment investigating addition order among the bS0.025-90/200 sample from the experiment investigation crystallisation order and the standard C-SAPO-5 was chosen for further analysis. An overview of results presented so far for these samples is given in Table 4.7, showing relative crystallinity, BET surface area and micro- and mesopore volume.

Table 4.7: Summary of results for samples chosen for further analysis, giving relative crystallinity, BET area and micropore and mesopore volumes.

Sample name	Crystallinity (%)	BET area (m^2/g)	Micropore vol. (cm^3/g)	Mesopore vol. (cm^3/g)
C-SAPO-5	100	218	0.08	0.04
aG0.025(24)-200	100	271	0.10	0.05
aS0.025(24)-200	108	248	0.10	0.03
bS0.025-90/200	75	178	0.07	0.08

The diffractograms of the chosen samples are given in Figure 4.18, all samples were phase pure except sample bS0.025-90/200 exhibiting some Tridymite impurity.
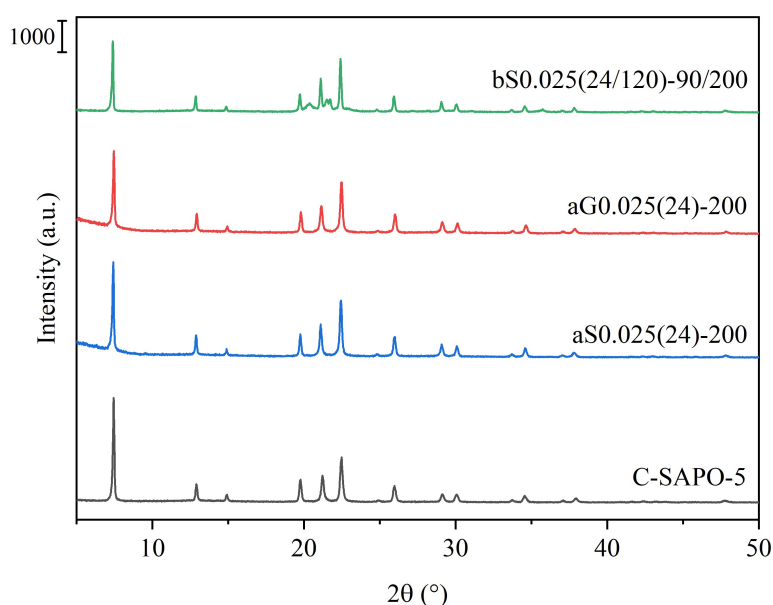

Figure 4.18: Diffractograms of samples chosen for further analysis.

4.8   Scanning electron microscopy

SEM imaging was conducted on the samples to investigate particle morphology and to calculate average particle size. In Figure 4.19, images of all four samples are shown with a magnification of approximately 8×2500, showing a typical particle found in each sample. The C-SAPO-5 particle displays spherical aggregates of rod-like particles which are in accordance with literature [21], however plate-like hexagonal and quadratic crystals are also observed in the sample which can be caused by the Si atoms [12]. Both samples from Synthesis A, sample aG0.025 and aS0.025 display particles that are cylindrical aggregates of platelets. The particle captured of sample bS0.025 also appears spherical in shape and also seemed to be aggregates of platelets, better observed in other particles, see Figure 4.20.d.

Figure 4.19: SEM images of C-SAPO-5 (a), aS0.025(24)-200 (b), aG0.025(24)-200 (c) and bS0.025(24/120)-90/200 (d) with magnification of 8×2500, showing a typical particle of the sample.

Both samples from Synthesis A have high monodispersity of particle size as shown in Figure 4.20.b-c and had relatively low standard derivations from the calculated particle size. Synthesis B displayed a wide range of particle sizes and it looks like the particles perhaps had dissolved, see Figure 4.20d. The particles that appeared spherical and intact were relatively equal in size, however particles with different

shapes were of different sizes. The spherical particles in the standard C-SAPO-5 samples also displayed high monodispersity.
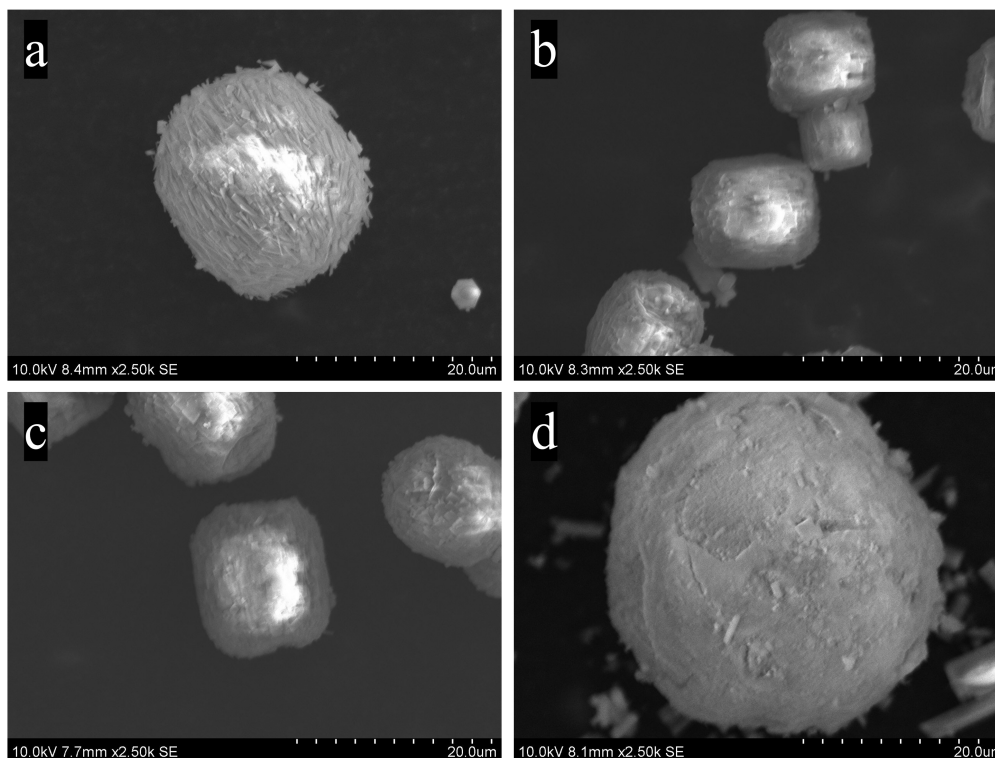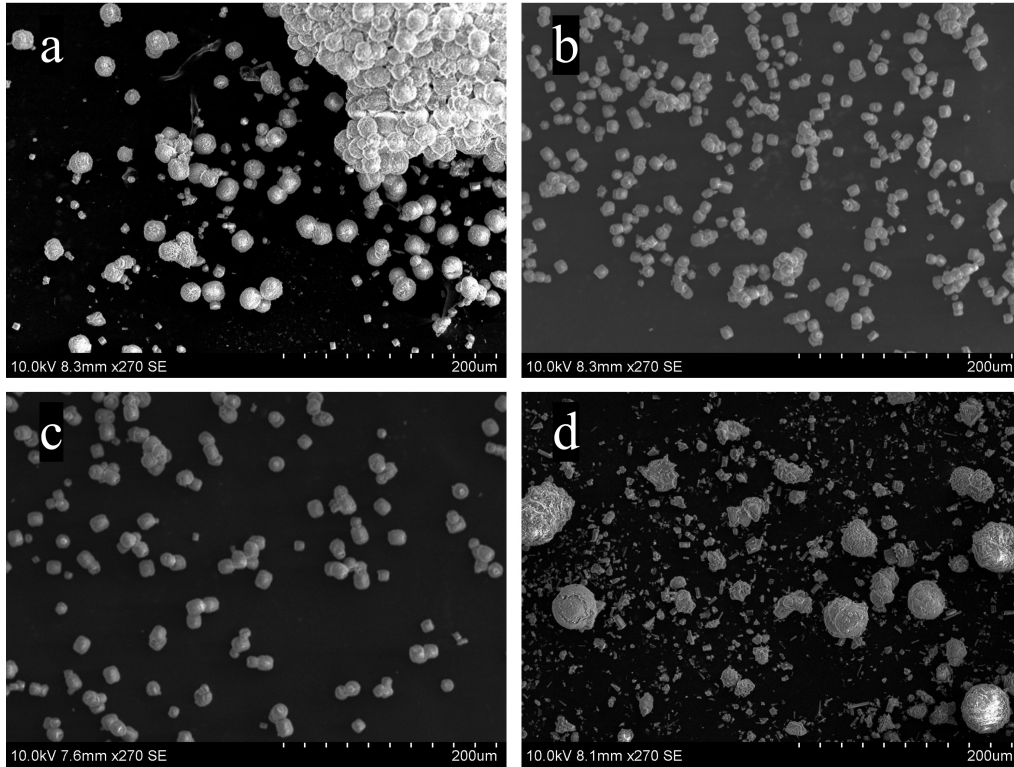

Figure 4.20: SEM images of C-SAPO-5 (a), aS0.025(24)-200 (b), aG0.025(24)-200 (c) and bS0.025(24/120)-90/200 (d) with magnification of 8×270, showing typical particle size distribution.

In Table 4.8 the average particle diameter was calculated from the images in 4.20 using 50 particles for each calculation that were chosen randomly. As the particles in samples aS0.025(24)-200 and aG0.025(24)-200 appeared cylindrical in shape, the diameter was measured along the rounded axis of the particle, to be consistent. For sample bS0.025(24/120)-200, only particles that looked above 10 µm were included in the calculations.

Table 4.8: Image analysis done with ImageJ of SEM images in Figure 4.20, showing average particle diameter in µm with standard derivation for each sample.

Sample name	Average particle diameter (µm))
C-SAPO-5	18.6 ± 2.2
aG0.025(24)-200	13.6 ± 1.5
aS0.025(24)-200	10.8 ± 0.8
bS0.025(24/120)-90/200	22.2 ± 10.2

The calculated average particle size for C-SAPO-5 at 18.6 µm which was in accordance with literature [11, 20, 21], and with a standard deviation of 2.2 µm again indicating monodispersity. The two samples from Synthesis A gave a significantly lower average diameter of 13.6 µm for glucose and 10.8 µm for sucrose. The standard deviation for these samples was also very low indicating the high monodispersity. The sample from Synthesis B gave the highest average diameter at 22.2 µm and had a high standard deviation of 10.2 µm. The spherical particles that appeared intact were mostly measured to around 30 µm, however the smaller particles lowered the average.

4.9   Fourier-transform infrared spectroscopy

FT-IR analysis was conducted to evaluate the acid sites and precursor hydroxyls in each sample. The normalized FT-IR spectra are given in Figure 4.21, which were measured at 300°C after dehydration at 550°C. As shown in the figure, distinct bands were observed for all samples corresponding to the bands found in literature [60], acid sites in the 6-membered-ring at 3428 - 3575 cm^{-1o}, acid sites in the 12-membered-ring at 3575 - 3653 cm^{-1}, P-OH at 3653 - 3690, Si-OH at 3690 - 3753 cm^{-1} and Al-OH at 3753 - 3808 cm^{-1} although these bands had low absorbance.
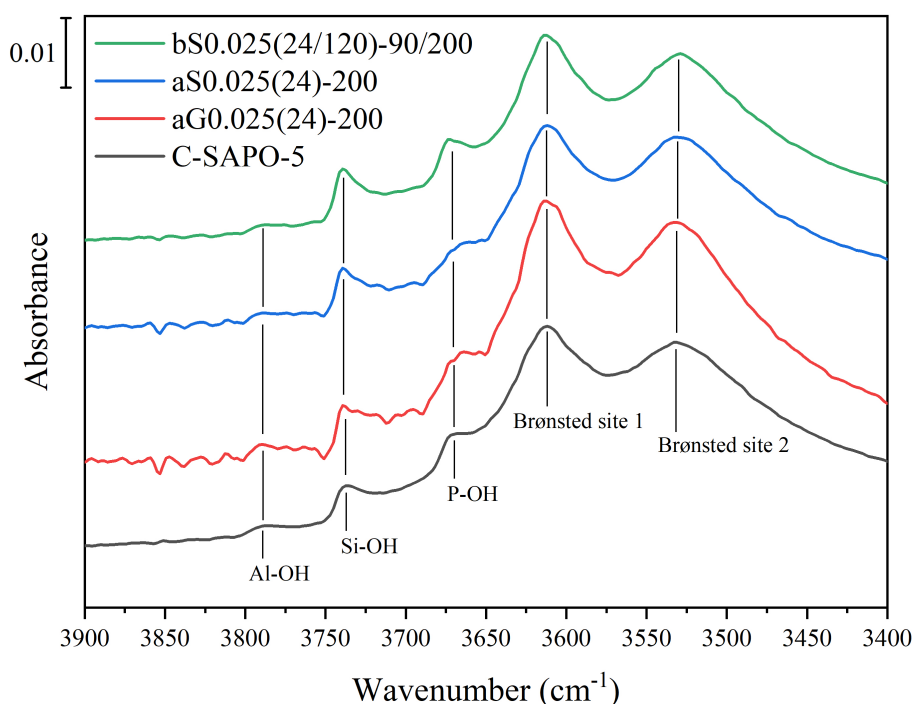

Figure 4.21: Normalised FT-IR spectra of samples measured 300°C.

The relative amounts of each hydroxyl were calculated using C-SAPO-5 as a standard, and the amounts are given in Table 4.9 below.

Table 4.9: Results from calculating relative amounts with FT-IR analysis, showing region on the spectra used for each hydroxyl and the amounts for each sample.

Band	Region (cm^{-1})	Relative amounts			
		C-SAPO-5	aG0.025	aS0.025	bS0.025
Brønsted site 2	3428 - 3575	1.00	1.41	1.11	1.17
Brønsted site 1	3575 - 3653	1.00	1.43	1.08	1.09
P - OH	3653 - 3690	1.00	1.70	0.86	1.62
Si - OH	3690 - 3753	1.00	1.89	1.67	1.74
Al - OH	3753 - 3808	1.00	3.69	1.81	0.63

The calculated relative amounts for acid sites and Al, Si and P hydroxyl are plotted in Figure 4.22, where all the hierarchical samples display a higher amount than the standard. The relative amounts of 12-membered-ring acid sites were highest for sample aG0.025 at 1.43, while samples aS0.025 and bS0.025 showed only a slight increase of 1.08 and 1.09 respectively.
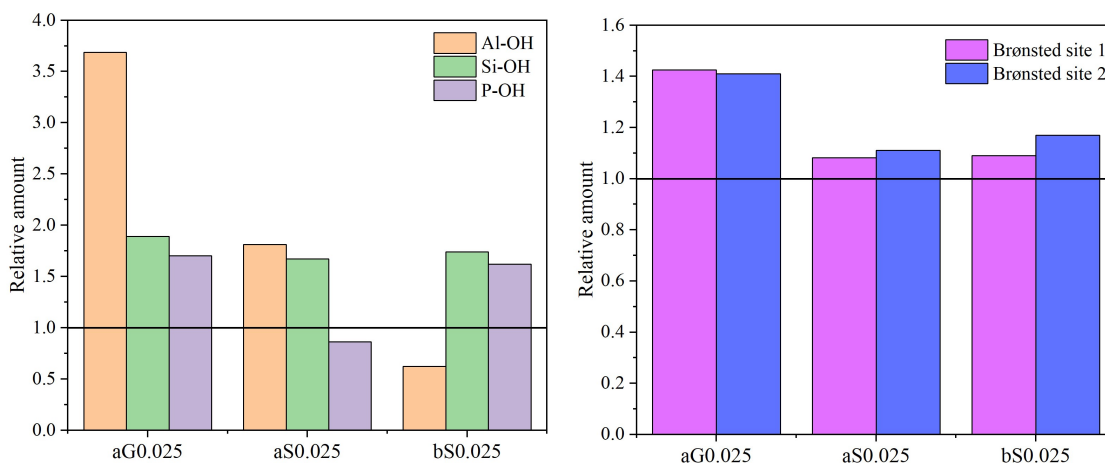
Figure 4.22: Calculated relative amounts, showing Al, Si and P hydroxyls on the left and Brønsted acid sites on the right.

The relative amounts of acid sites also increase in an order of aS0.025 < bS0.025 < aG0.025 for the 6-membered-ring sites, and correlates to the Si-OH amount where aG0.025 has the highest relative amount at 1.89, almost double the amount of the standard, followed by 1.74 for bS0.025 and 1.67 for aS0.025. As the amount of acid sites is dependent on the silicon, this relationship is expected.

5   Discussion

The main goal for this thesis was to successfully synthesise hierarchical SAPO-5 using glucose and sucrose as sustainable meso-SDAs. The level of success was determined by the characterisation of the samples where a phase pure sample exhibiting high crystallinity, sufficient BET surface area, and pore volumes as desired. Initially, the main findings will be discussed in three parts where the synthesis, meso-SDAs and pore hierarchy are evaluated before a conclusion is drawn.

5.1   Using saccharides as meso-SDA

As described in the theory section, saccharides have not been thoroughly studied in use as meso-SDAs for SAPO-5, and its use for dual templating is a relatively new section of synthesis of hierarchical materials. It is therefore a natural continuation to do a thorough evaluation of the use of sucrose and glucose, which have been studied as meso-SDA in this thesis. Four main observations regarding porosity, crystallinity, particle size and acidity, have emerged when looking at the results in comparing the use of the two saccharides to synthesise hierarchical SAPO-5, which will be discussed in the following chapter.

In the results from nitrogen physisorption, it appeared that higher levels of glucose in the samples consistently resulted in higher BET surface area for samples with Synthesis A. The interesting observation with this trend is that the increase in surface area was seen in the micropore area rather than the external. As the external surface area represents the mesopore area of the material [49, 50], it would be expected that this area would increase with a higher ratio of glucose, as has been reported in literature where Nandan et al. found that the hierarchical porosity of ZSM-5 was enhanced by increasing the amount of glucose used in synthesis [44]. However, this was not the case for the glucose samples in this thesis, thus suggesting an explanation for the trend is difficult. It seemed that the increased micropore surface area corresponds to a similar trend where micropore volume increased with an increased glucose ratio. Again, the increase is not observed for the mesopore volume, suggesting that the glucose solution had a positive effect on the assembly of micropores in the synthesis gel solution, rather than producing more mesopores in the material. The trend is again not observed for sucrose samples, suggesting that the effect is unique for glucose. In Synthesis B however, both glucose and sucrose resulted in a significantly higher mesopore volume, though it is difficult to ascertain if the effect was caused by the saccharides as a standard microporous sample was not synthesised with this addition order. The two samples with Synthesis B exhibited

a significantly lower BET surface area and despite this, mesopore volumes were closer to what is found in literature for hierarchical samples compared to Synthesis A samples.

For synthesis B samples, relative crystallinity did not significantly differ between glucose and sucrose in the first experiment, although glucose was slightly higher at 65% versus 52% for sucrose. However, in the second experiment investigating crystallisation time, sucrose proved itself superior to glucose as it resulted in higher crystallinities at longer crystallisation times. As previously discussed, the low outcomes from this experiment could have been caused by the low crystallisation temperature, and therefore glucose could also display similar results with a pre-crystallisation step. However, this can only be proved with further synthesis work which was not possible within the time frame of this thesis. Therefore, by the results presented here, sucrose was deemed the best meso-SDA for synthesis B.

The most interesting observation from SEM analysis was that the particles from samples aS0.025 and aG0.025 were significantly smaller than the standard microporous sample, with average particle diameters of 10.8 and 13.6 µm respectively, compared to the average particle diameter of C-SAPO-5 at 18.6 µm. It seemed that for Synthesis A both sucrose and glucose worked as surfactants that restricted the particle size, thus producing smaller particles with a cylindrical shape rather than the expected spherical. This effect has been reported for more conventional meso-SDAs, such as C-TAB that controls particle size in the synthesis of zeotypes [21, 67]. Interestingly, in Synthesis B, sucrose did not lower the particle size but rather produce larger particles. Furthermore, the formation of aggregates of some SAPO catalysts is due to longer crystallization time, [68], which could explain why the particles in the Synthesis B samples looked dissolved as it was crystallised for 120 hours. As a final comment on particle size, the high surface areas of the Synthesis A samples would perhaps be explained by the smaller particle size, however as the external surface area did not increase significantly from sample C-SAPO-5, this observation is hard to interpret. If time had allowed, analysing all glucose and sucrose samples from Synthesis A with SEM would elucidate if higher ratios of meso-SDA would give smaller particles, thus adding to the observed trend for this addition order. As sucrose gave smaller particles with synthesis A and larger particles with Synthesis B, suggesting that the surfactant effect is caused by the synthesis addition order.

When evaluating the results from FT-IR analysis, it seemed that glucose was superior in promoting Brønsted acid sites as the highest relative amount of 1.43 in the

12-membered ring was found in sample aG0.025, which used glucose as meso-SDA. This sample also had the highest BET surface area of the four samples analysed, however, had the same micropore volume as aS0.025, suggesting that glucose promoted the formation of acid sites in the micropores, or perhaps promoted acid sites in the mesopores. This however can only be investigated with further catalytic analysis of the acid sites. As a high amount of acid site is correlated to the Si/Al ratio of the material, one would therefore expect sample aG0.025 to exhibit a higher ratio. This was not the case as sample aG0.025 had a Si/Al ratio at 0.15, which lay in between sample aS0.025 at 0.16 and bS0.025 at 0.13, and is therefore inconclusive. As for sucrose, approximately the same relative amount of Brønsted acid sites was found in samples aS0.025 and bS0.025, suggesting that the type of meso-SDA influenced the acidity rather than the synthesis addition order.

5.2   Evaluating the pore hierarchy

Perhaps the most important aspect of the results is to evaluate whether the samples synthesised can be considered as hierarchical SAPO-5 as it was the desired product for the thesis. A hierarchical sample should exhibit a degree of hierarchy, while there are many different ways of defining pore hierarchy, such as calculating the Hierarchical Factor [69], they are not necessarily representative of all hierarchical materials. The Hierarchical Factor for all the samples synthesised in this thesis is given in Table 9.1, however the values will not be discussed. Nevertheless, as mentioned earlier in this thesis, hierarchical SAPO-5 almost always exhibit a mesopore volume equal to or higher than the micropore volume [7, 21, 66], and this will therefore be the primary requirement for this evaluation.

Samples from Synthesis A all exhibit a good surface area and micropore volume that meets the expected value from literature. However, all the samples exhibit a mesopore volume of less than half the value of the micropore volume. According to the requirement presented above these samples from Synthesis A would therefore not be considered hierarchical. On the other hand, looking at the physisorption isotherms of the samples we see that all exhibit hysteresis loops, which is a clear indication of the presence of mesopores. Together with the distinct shoulders featured in most of the PSD distribution curves, one might suggest that there is in fact some degree of hierarchy due to the presence of mesopores in the samples from Synthesis A.

Samples from Synthesis B, as already discussed, exhibited significantly higher mesopore volumes than the samples from Synthesis A, due to the synthesis addition or-

der. Sample bG0.025(24)-200 exhibited a relatively high mesopore volume of 0.13 cm^3/g and a low micropore area of 0.05 cm^3/g, which is similar to the values found for hierarchical SAPO-5 produced in the article by Mariatti et. al. from which Synthesis B is based on [47]. By their definitions, such pore volumes would define the bG0.025 sample as hierarchical, if it were not for the low surface area of 147 m^2/g, the Tridymite impurity and the low relative crystallinity of 63%. Notably however, the Hierarchical Factor is applied to the sample of Mariatti et. al., it would be considered mesoporous materials rather than hierarchical.

Sample bS0.025(24/120)-90/200 also exhibited a BET surface area lower than literature values at 178 m^2/g and has a high relative crystallinity at 75% and exhibits a significantly lower Tridymite phase. The pore volumes in this sample do in fact resemble the ratio expected from hierarchical SAPO-5 in literature, showing 0.07 and 0.08 cm^3/g for micro- and mesopore volume respectively. These volumes are somewhat lower than what is found in literature, however this could be caused by the low BET surface area. Therefore it seems prudent to assume that this sample is in fact hierarchical, and would be the most successful sample from this project.

5.3   Optimal synthesis for hierarchical SAPO-5

In this thesis, different synthesis parameters were varied to study their effect on synthesising hierarchical SAPO-5. The addition order and crystallisation time and temperature gave varying results that will be discussed in this section.

To study the effect of synthesis addition order, two different synthesis addition orders were conducted, referred to as Synthesis A and B. Synthesis A added the elements in the order of P, Al, Si, TEA and then meso-SDA, while Synthesis B had the order of Al, TEA, Si, meso-SDA and finally P at the end. The two most significant differences in the synthesis addition order are based on observations found in literature. One of them is that TEA is added earlier in the synthesis, and secondly, that mesa-SDA is added before the phosphorous.

As for the silicon content, in a traditional hydrothermal synthesis of SAPO-5 the aluminium, phosphorous and silicon precursors, the template and water are added together in a certain order and mixed to create a solution gel. The addition order for the synthesis of SAPO-5 varies to some degree, however, it seems like the initial addition of the aluminium and phosphorus precursors is the superior method to produce phase-pure and high-quality materials, both microporous and hierarchical [7, 20, 21]. It is however not consistent in literature whether the micro-SDA or

silicon precursor is added first, where Mathisen et. al. used a method where the Si source was added after Al, P and water, followed by the addition of the template [70] as described by Synthesis A used in this thesis. In other works, the micro-SDA was added before the Si source [7, 20, 47], which corresponds to the addition order of Synthesis B, where samples in the works did not exhibit any significant difference in quality. These findings from literature suggest that the addition order of Si and micro-SDA do not have any significant effect on the quality of the produced SAPO-5. This was demonstrated in the results, where Si content did not significantly change from Synthesis A, where Si was added before TEA, to Synthesis B, where Si was added after. The relative amounts of Si-OH calculated from FT-IR showed that the sample bS0.025(24/120)-90/200 had a value that laid in between the two samples aS0.025 and aG0.025, and in ICP-MS analysis, Si/Al ratio did not decrease significantly more in either synthesis addition order.

Regarding the mesopore volume, Yang et. al. [46] did an extensive study on the synthesis of hierarchical AlPO-5 using saccharides as meso-SDAs. They investigated the effect of addition order on the amount of mesopore volume in their materials, and synthesised materials where the meso-SDA was added at various stages of the synthesis order. Starting with a general recipe with an addition order of aluminium source with water, phosphorus source, then TEA, they added the meso-SDA at three different stages, after Al, after P or after TEA. After the characterisation of the materials, two interesting observations were illuminated. Firstly, they found that if the micro-SDA used, TEA, was added before the glucose used as meso-SDA, more mesopores were produced. They argued that because TEA as an SDA is basic in nature, and therefore promoted the formation of negative charges on the aluminumphosphate structure. These negative charges could then act as hydrogen bond acceptors for the hydroxyl groups on the glucose molecules leading to more glucose in the solution gel and more mesopores in the final product. Yang et. al. also found that by adding the glucose before the phosphorus precursor, even more mesopores were produced. They suggested that this was due to the protons in the phosphoric acid competing with the hydroxyl groups on the glucose for the negative charges on pseudoboehmite, the alumina precursor [46]. Synthesis B reflects both of these observations, as TEA was added right after the Al, and meso-SDA was added before P. It is therefore quite notable that when comparing Synthesis A and B, the latter produced a significantly higher mesopore volume, suggesting that these hypotheses given by Yang et. al. for hierarchical AlPO-5 were also relevant for the synthesis of hierarchical SAPO-5 using glucose and sucrose as meso-SDA.

Although the mesopore volume produced in Synthesis B corresponded well to this literature, it is important to note that all its samples exhibited some degree of impurities, and significantly lower crystallinities compared to Synthesis A. All the samples from Synthesis A were phase pure and exhibited relative crystallinities close to 100%. Other results such as BET surface area and micropore volume were similar to literature values for Synthesis A, while samples from Synthesis B displayed lower values than expected, however these results will be further discussed in the evaluation of pore hierarchy.

Regarding the phosphorous content, the hypothesis of Yang et. al. would perhaps suggest that samples from Synthesis B, where the phosphorous is added at the end, would exhibit a lower level of P in the material as the phosphoric acid competes with the glucose. However, this was not the case from the results in ICP-MS, where sample bS0.025 had the highest P wt.% of all samples at 26.6, see Table 10.1, showing that Synthesis B was in fact successful in incorporating both mesopores and phosphorous.

Another synthesis parameter that was studied in this thesis was the crystallisation time in an attempt to diminish the Tridymite impurities produced in Synthesis B, as longer crystallisation time has been reported in the literature to promote the SAPO-5 phase AFI in hydrothermal synthesis [71]. The results from this experiment showed that the synthesis had an optimal crystallisation time for sucrose samples of 96 hours for AFI crystallinity and 120 hours for diminishing the Tridymite phase. At longer crystallisation times, the Tridymite phase increased and relative crystallinity fell. As the goal was to find a crystallisation time best for phase purity, 120 hours was chosen for further experiments, despite the observation that the bS0.025(24)-200 sample from the experiment investigating addition order displayed a lower Tridymite phase than the bS0.025(120)-150 sample, and the relative crystallinity was slightly lower in the bS0.025(96)-150 sample compared to sample bS0.025(24)-200, 47% contra 52%. This would perhaps suggest that the experiment investigating crystallisation time was not successful as the results were not improved from the bS0.025(24)-200 sample. On the other hand, crystallisation temperature was not the same for these two experiments and comparing the samples based on time is not advisable as temperature could have contributed to a decline in phase purity and crystallinity. The temperature used in this experiment was 150°C, and as the results from the next experiment show, crystallisation at 200°gave a significantly higher relative crystallinity than 150°C. The conclusions drawn from this experiment should therefore be considered valid findings for the effect of crystallisation

time.

The last synthesis parameter that was studied in this thesis was crystallisation temperature. The results of Synthesis B have thus far given the impression that Tridymite impurities cannot be successfully diminished by increasing the crystallisation time, as the sample crystallised at 120 hours still exhibited some degree of Tridymite phase and the answer might be found in altering the temperature. As observed from all hierarchical synthesis, glucose and sucrose decompose during crystallisation. A temperature trial was therefore conducted to find the point of decomposition for glucose and sucrose that gave a possible decomposition temperature between 120 and 100°C, suggesting that a crystallisation temperature in between these temperatures is required to avoid the decomposition of meso-SDA. However in literature, the synthesis of SAPO-5 is reported to only be possible above a crystallisation temperature of 150°C [11]. Endregard et. al. investigated the hydrothermal synthesis of AlPO-5 with incorporated cobalt (Co). In their paper, they describe the crystallisation with a preheating step of the stainless-steel "bomb" as it was heated at autogenous pressure to 90°C for 22 hours before it was heated to 200°C for 27 hours [61]. Ageing at higher temperatures can increase the phase purity of the sample. Agliullin et. al. found that ageing their gel at 90°C for 24 hours before crystallisation, improved the fraction of the amorphous phase for SAPO-11 [72]. Using a low-temperature pre-crystallisation heating step would perhaps allow the sucrose to be properly set in the synthesis gel before undergoing further crystallisation. The results from this pre-crystallisation step were quite promising, where the sample with 0.025 sucrose ratio gave a significantly higher relative crystallinity with considerably less Tridymite impurity. As mentioned earlier, this sample also exhibited a high mesopore volume and the best pore hierarchy.

In summary, both Synthesis A and B result in hierarchical SAPO-5, however with a varying degree of hierarchy. Synthesis A produced phase pure samples with higher crystallinity, BET surface area and higher micropore volume, while Synthesis B produced higher mesopore volume and degree of hierarchy. The optimum synthesis parameters seemed to involve a longer crystallisation time to lower the Tridymite impurities and a pre-crystallisation for a higher AFI framework with mesopores. It would therefore be interesting to combine the Synthesis A addition order with these parameters to achieve a sample with higher BET surface area and micropore volume, and perhaps a longer crystallisation time is not necessary as Synthesis A did not exhibit Tridymite impurities. This combination should be conducted with glucose the highest relative amount of acid sites was achieved with this template.

6   Conclusion

Hierarchical SAPO-5 has in varying degrees been successfully synthesised with the use of sustainable meso-SDA. Hierarchical samples were produced with both Synthesis A and B, where Synthesis A samples showed clear hysteresis loops in the isotherms and some degree of mesopore uniformity in the form of features of the PSD, and the samples were deemed as hierarchical with a low hierarchy. A superior hierarchical sample was produced with Synthesis B, where pore volumes suggested a high degree of hierarchy.

From the parameter study conducted, it seemed like the optimal synthesis for producing hierarchical SAPO-5 would involve the addition order of Synthesis B, where meso-SDA was added before the phosphorous precursor, for producing mesopores, using a higher crystallisation time for diminishing Tridymite phase and including a pre-crystallisation step to increase the crystallinity of AFI phase. Comparing the type of meso-SDA used suggested that sucrose was the superior template in the optimal synthesis described above, while glucose was superior for promoting acid sites in the material. Both sucrose and glucose produced smaller particles for Synthesis A.

In conclusion, glucose and sucrose can be used as meso-SDA for the synthesis of hierarchical SAPO-5, though further adjustments should be researched to achieve better results.

7   Further research

To begin with, it seems reasonable to undergo further catalytic testing of the three hierarchical samples chosen for further research, to investigate the interconnectivity of the pore systems and to further evaluate the location of the acid site, as described in the study done by Ali et. al. [21].

As mentioned in the discussion, it would also be interesting to do SEM imaging of all the glucose and sucrose samples with Synthesis A, to elucidate whether a higher meso-SDA ratio would result in smaller particles.

As Synthesis A gave good XRD and BET surface area results, and the pre crystallisation step added to Synthesis B resulted in a good hierarchy, it would perhaps be interesting to synthesise a new sample with the addition order of Synthesis A and the pre-crystallisation step to see if the combination might result in an even better hierarchical SAPO-5.

Starch has shown great promise as meso-SDA in the synthesis of hierarchical ZSM-5, where a high mesopore volume was achieved [42]. It would be fascinating to test the optimal synthesis parameters found in this thesis with other sustainable meso-SDAs such as starch.

References

[1] H. Ritchie, M. Roser, P. Rosado, *Our world in data* **2020**.

[2] K. Zhang, U. Kogelschatz, B. Eliasson, *Energy & fuels* **2001**, *15*, 395–402.

[3] Y. Li, L. Li, J. Yu, *Chem* **2017**, *3*, 928–949.

[4] F. Bauer, J. P. Tilsted, S. Pfister, C. Oberschelp, V. Kulionis, *Current Opinion in Chemical Engineering* **2023**, *39*, 100881.

[5] P. W. Griffin, G. P. Hammond, J. B. Norman, *Applied Energy* **2018**, *227*, Transformative Innovations for a Sustainable Future – Part III, 587–602.

[6] P. T. Anastas, J. C. Warner, *Green chemistry: Theory and practice* **1998**, *29*.

[7] N. Danilina, F. Krumeich, J. A. van Bokhoven, *Journal of Catalysis* **2010**, *272*, 37–43.

[8] Molecular sieve definition amp; meaning.

[9] Z.-A. Qiao, Q.-S. Huo in *Modern Inorganic Synthetic Chemistry (Second Edition)*, (Eds.: R. Xu, Y. Xu), Elsevier, Amsterdam, **2017**, pp. 389–428.

[10] X. Chen, G. Yang, V. Valtchev, *Green Energy Environment* **2020**, *5*, Green Catalysis and Kinetics, 394–404.

[11] H. Weyda, H. Lechert, *Zeolites* **1990**, *10*, 251–258.

[12] K. Utchariyajit, S. Wongkasemjit, *Microporous and mesoporous materials* **2010**, *135*, 116–123.

[13] AFI: Type Material - Structure Commission of the International Zeolite Association, `https://asia.iza-structure.org/IZA-SC/material_tm.php?STC=AFI`, [Accessed 17-Aug-2022], **2007**.

[14] O. Cheung, Q. Liu, Z. Bacsik, N. Hedin, *Microporous and Mesoporous Materials* **2012**, *156*, 90–96.

[15] S. Hedge, P. Ratnasamy, L. Kustov, V. Kazansky, *Zeolites* **1988**, *8*, 137–141.

[16] R. Roldán, M. Sánchez-Sánchez, G. Sankar, F. J. Romero-Salguero, C. Jiménez-Sanchidrián, *Microporous and Mesoporous Materials* **2007**, *99*, 288–298.

[17] J. Weitkamp, *Solid State Ionics* **2000**, *131*, 175–188.

[18] P. Atkins, T. Overton, J. Rourke, M. Weller, F. Armstrong, *Shriver and Atkins' inorganic chemistry*, 5th ed., Oxford University Press, London, England, **2009**.

[19] S. ul Hasnain Bakhtiar, S. Ali, Y. Dong, X. Wang, F. Yuan, Z. Li, Y. Zhu, *Journal of Porous Materials* **2018**, *25*, 1455–1461.

[20] A. F. Ojo, J. Dwyer, J. Dewing, P. J. O'Malley, A. Nabhan, *J. Chem. Soc., Faraday Trans.* **1992**, *88*, 105–112.

[21] D. Ali, C. R. Zeiger, M. M. Azim, H. L. Lein, K. Mathisen, *Microporous and Mesoporous Materials* **2020**, *306*, 110364.

[22] Z. Zhu, Q. Chen, Z. Xie, W. Yang, C. Li, *Microporous and Mesoporous Materials* **2006**, *88*, 16–21.

[23] U. Sridevi, *Petroleum Refining and Petrochemical Based Industries in Eastern India.* **2000**, 89.

[24] S. H. Jhung, J.-S. Chang, J. S. Hwang, S.-E. Park, *Microporous and Mesoporous Materials* **2003**, *64*, 33–39.

[25] M. M. Azim, A. Stark, *ChemistrySelect* **2018**, *3*, 12495–12503.

[26] R. E. Morris, *Chem. Commun.* **2009**, 2990–2998.

[27] S.-H. Feng, G.-H. Li in *Modern Inorganic Synthetic Chemistry (Second Edition)*, (Eds.: R. Xu, Y. Xu), Elsevier, Amsterdam, **2017**, pp. 73–104.

[28] C. S. Cundy, P. A. Cox, *Microporous and Mesoporous Materials* **2005**, *82*, 1–78.

[29] A. R. West, *Solid State Chemistry and its Applications*, 2nd ed., John Wiley & Sons, Nashville, TN, **2014**.

[30] G. Cao, Y. Wang, *Nanostructures and Nanomaterials*, **2022**.

[31] A. H. Chowdhury, N. Salam, R. Debnath, S. M. Islam, T. Saha in *Nanomaterials Synthesis*, (Eds.: Y. Beeran Pottathara, S. Thomas, N. Kalarikkal, Y. Grohens, V. Kokol), Micro and Nano Technologies, Elsevier, **2019**, pp. 265–294.

[32] Y. Ji, Y. Wang, B. Xie, F.-S. Xiao, *Comments on Inorganic Chemistry* **2016**, *36*, 1–16.

[33] M. Marcos-Hernández, D. Villagrán in *Composite Nanoadsorbents*, (Eds.: G. Z. Kyzas, A. C. Mitropoulos), Micro and Nano Technologies, Elsevier, **2019**, pp. 265–293.

[34] A. Feliczak-Guzik, *Microporous and Mesoporous Materials* **2018**, *259*, 33–45.

[35] V. Solano, J. Vega-Baudrit, *Journal of Biomaterials and Nanobiotechnology* **2015**, *6*, 247–256.

[36] C. H. Christensen, K. Johannsen, E. Törnqvist, I. Schmidt, H. Topsøe, C. H. Christensen, *Catalysis Today* **2007**, *128*, Catalytic Nano-Oxides Research and Development in Europe: Present and Future (Final CONCORDE Conference), Seville, Spain, 16-19 May 2006, 117–122.

[37] X. Jia, W. Khan, Z. Wu, J. Choi, A. C. Yip, *Advanced Powder Technology* **2019**, *30*, 467–484.

[38] J. W. Niemantsverdriet, *Spectroscopy in Catalysis*, Wiley, **2007**.

[39] J. Pérez-Ramırez, C. H. Christensen, K. Egeblad, C. H. Christensen, J. C. Groen, *Chemical Society Reviews* **2008**, *37*, Image republished with permission of The Royal Society of Chemistry, from Hierarchical zeolites: enhanced utilisation of microporous crystals in catalysis by advances in materials design, Pérez-Ramırez et. al. (Royal Society of Chemistry), 37, Issue 11, 2008; permission conveyed through Copyright Clearance Center, Inc. Licence ID: 1302151-1., 2530–2542.

[40] M. Hartmann, A. G. Machoke, W. Schwieger, *Chemical Society Reviews* **2016**, *45*, 3313–3330.

[41] Q. Che, M. Yang, X. Wang, Q. Yang, Y. Chen, X. Chen, W. Chen, J. Hu, K. Zeng, H. Yang, H. Chen, *Bioresource Technology* **2019**, *289*, 121729.

[42] A. Maghfirah, M. Ilmi, A. Fajar, G. Kadja, *Materials Today Chemistry* **2020**, *17*, 100348.

[43] L. Jin, T. Xie, S. Liu, Y. Li, H. Hu, *Catalysis Communications* **2016**, *75*, 32–36.

[44] D. Nandan, S. K. Saxena, N. Viswanadham, *Journal of Materials Chemistry A* **2014**, *2*, 1054–1059.

[45] Z. Liu, L. Liu, H. Song, C. Wang, W. Xing, S. Komarneni, Z. Yan, *Materials Letters* **2015**, *154*, 116–119.

[46] X. Yang, T. Lu, C. Chen, L. Zhou, F. Wang, Y. Su, J. Xu, *Microporous and Mesoporous Materials* **2011**, *144*, 176–182.

[47] F. Mariatti, I. Miletto, G. Paul, L. Marchese, S. Tabasso, M. Manzoli, G. Cravotto, E. Gianotti, *RSC Adv.* **2020**, *10*, 38578–38582.

[48] H. Stanjek, W. Häusler, *Hyperfine Interactions* **2004**, *154*, 107–119.

[49] K. S. W. Singh, J. Rouquerol, G. Bergeret, P. Gallezot, M. Vaarkamp, D. C. Koningsberger, A. K. Datye, J. W. Niemantsverdriet, T. Butz, G. Engelhardt, G. Mestl, H. Knzinger, H. Jobic in *Handbook of Heterogeneous Catalysis*, Wiley-VCH Verlag GmbH, pp. 427–582.

[50] P. A. Webb, C. Orr, *Analytical methods in fine particle technology*, Micromeritics Instrument Corporation, **1997**.

[51] M. Thommes, K. Kaneko, A. V. Neimark, J. P. Olivier, F. Rodriguez-Reinoso, J. Rouquerol, K. S. Sing, *Pure and Applied Chemistry* **2015**, *87*, 1051–1069.

[52] K. S. W. Sing, *Pure and Applied Chemistry* **1982**, *54*, 2201–2218.

[53] I. Chorkendorff, J. W. Niemantsverdriet, *Concepts of modern catalysis and kinetics*, 3rd ed., Wiley-VCH Verlag, Weinheim, Germany, **2017**.

[54] X.-L. Wei, X.-H. Lu, T.-J. Zhang, X. Chu, D. Zhou, R.-F. Nie, Q.-H. Xia, *Microporous and Mesoporous Materials* **2015**, *214*, 80–87.

[55] W. Lai, S. Yang, Y. Jiang, F. Zhao, Z. Li, B. Zaman, M. Fayaz, X. Li, Y. Chen, *Adsorption* **2020**, *26*, 633–644.

[56] S. Crouch, D. West, F. Holler, D. A. Skoog, *Fundamentals of analytical chemistry*, 9th ed., Brooks/Cole, Florence, KY, **2013**.

[57] R. Thomas, *Practical guide to ICP-MS*, 2nd ed., CRC Press, Boca Raton, FL, **2008**.

[58] H. E. Taylor, *Inductively coupled plasma-mass spectrometry: practices and techniques*, Academic press, **2001**.

[59] M. M. Beasley, E. J. Bartelink, L. Taylor, R. M. Miller, *Journal of Archaeological Science* **2014**, *46*, 16–22.

[60] F. Schüth, D. Demuth, B. Zibrowius, J. Kornatowski, G. Finger, *Journal of the American Chemical Society* **1994**, *116*, 1090–1095.

[61] M. Endregard, D. G. Nicholson, M. Stöcker, G. M. Lamble, *J. Mater. Chem.* **1995**, *5*, 785–791.

[62] X. Zhao, H. Wang, C. Kang, Z. Sun, G. Li, X. Wang, *Microporous and Mesoporous Materials* **2012**, *151*, 501–505.

[63] Y. Xiao, R. Kirkpatrick, Y. Kim, *Physics and Chemistry of Minerals* **1995**, *22*.

[64] W. Kang, Z. Zhang, *Catalysts* **2020**, *10*.

[65] J. A. Martens, P. J. Grobet, P. A. Jacobs, *Journal of Catalysis* **1990**, *126*, 299–305.

[66] M. E. Potter, L. N. Riley, A. E. Oakley, P. M. Mhembere, J. Callison, R. Raja, *Beilstein journal of nanotechnology* **2019**, *10*, 1952–1957.

[67] X. Wang, S. Ali, F. Yuan, Z. Li, Y. Zhu, et al., *Dalton Transactions* **2018**, *47*, 9861–9870.

[68] C. S. Punla, https://orcid.org/ 0000-0002-1094-0018, cspunla@bpsu.edu.ph, R. C. Farro, https://orcid.org/0000-0002-3571-2716, rcfarro@bpsu.edu.ph, Bataan Peninsula State University Dinalupihan, Bataan, Philippines, *International Multidisciplinary Research Journal* **2022**, *4*, 50–59.

[69] J. Pérez-Ramírez, D. Verboekend, A. Bonilla, S. Abelló, *Advanced Functional Materials* **2009**, *19*, 3972–3979.

[70] K. Mathisen, M. Stockenhuber, D. G. Nicholson, *Phys. Chem. Chem. Phys.* **2009**, *11*, 5476–5488.

[71] B. Valizadeh, S. Askari, R. Halladj, A. Haghmoradi, *Synthesis and Reactivity in Inorganic Metal-Organic and Nano-Metal Chemistry* **2014**, *44*, 79–83.

[72] M. R. Agliullin, Z. R. Khairullina, R. Z. Kuvatova, B. I. Kutepov, *Catalysis in Industry* **2020**, *12*, 89–94.
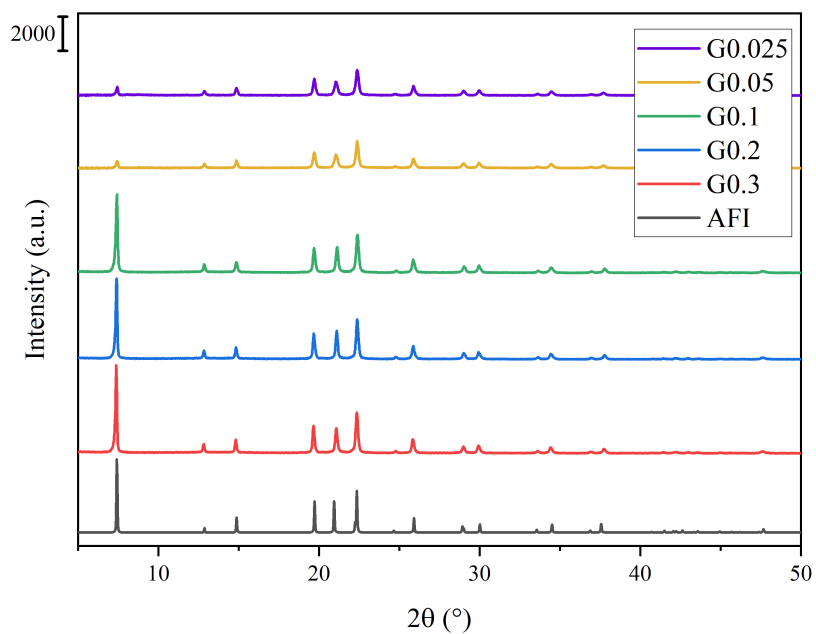
8   Appendix A - XRD

Figure 8.1: Diffractograms of as-prepared samples from experiment investigating addition order with Synthesis A, showing glucose samples.
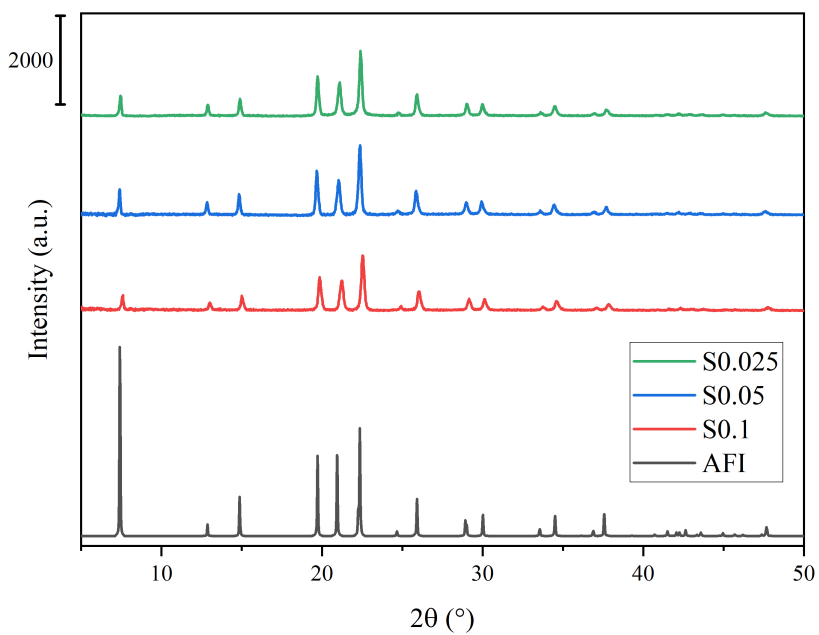

Figure 8.2: Diffractograms of as-prepared samples from experiment investigating addition order with Synthesis A, showing sucrose samples.
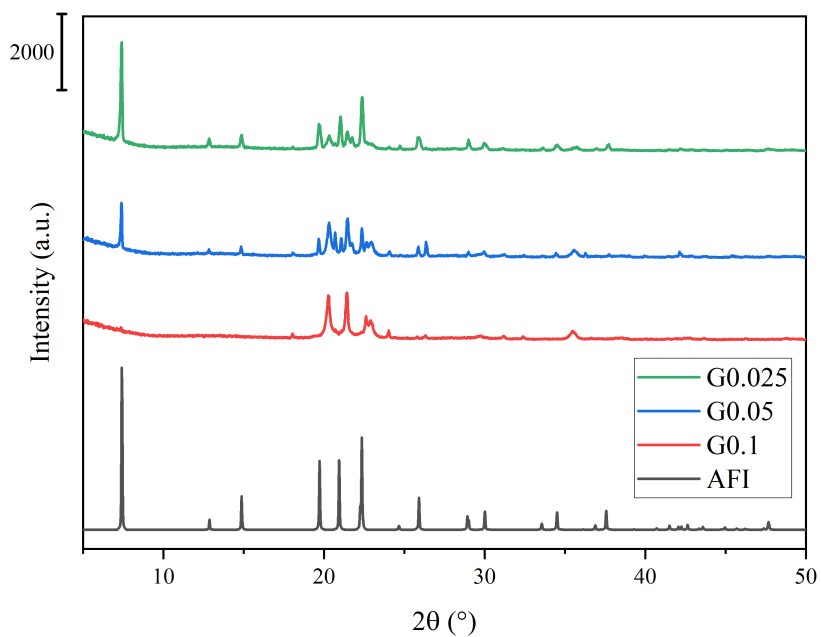
Figure 8.3: Diffractograms of as-prepared samples from experiment investigating addition order with Synthesis B, showing glucose samples.
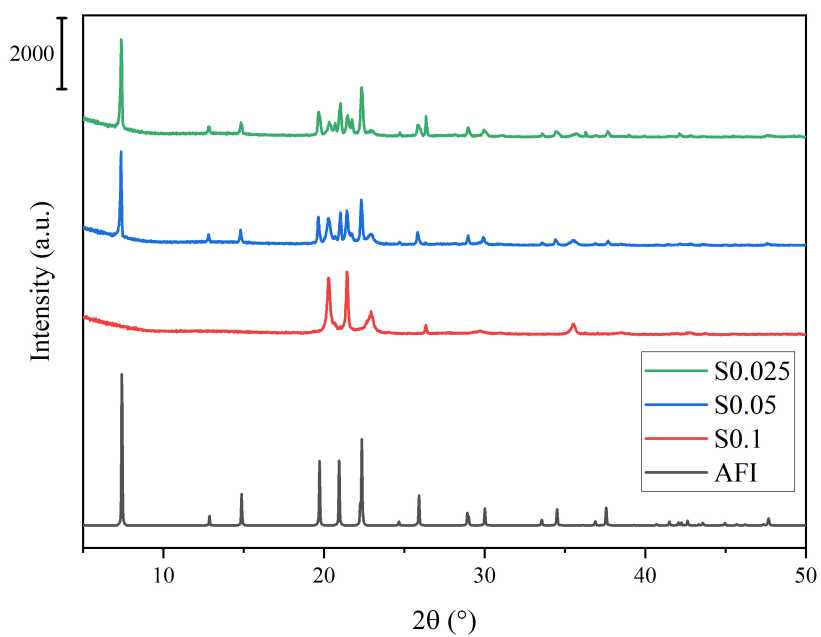

Figure 8.4: Diffractograms of as-prepared samples from experiment investigating addition order with Synthesis B, showing sucrose samples.
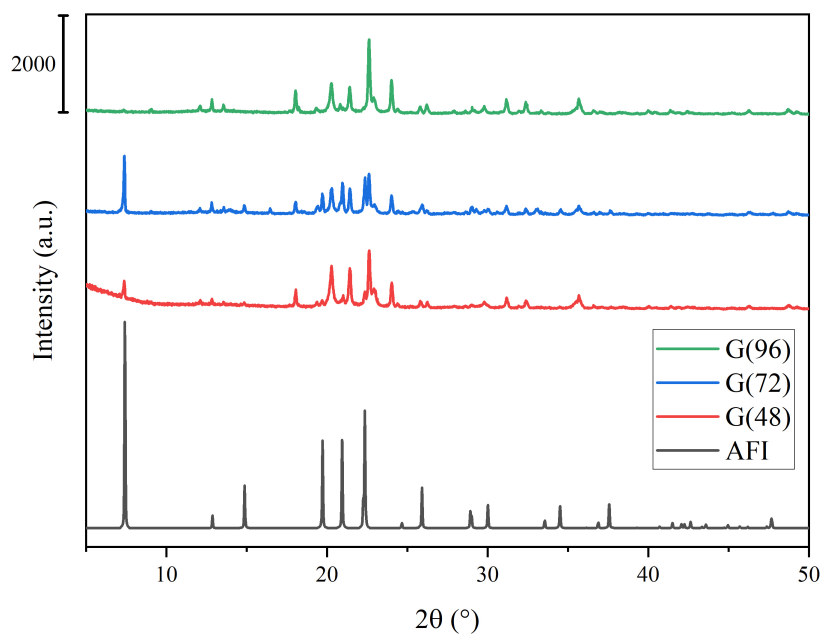
Figure 8.5: Diffractograms of as-prepared samples from experiment investigating crystallisation time, showing glucose samples.
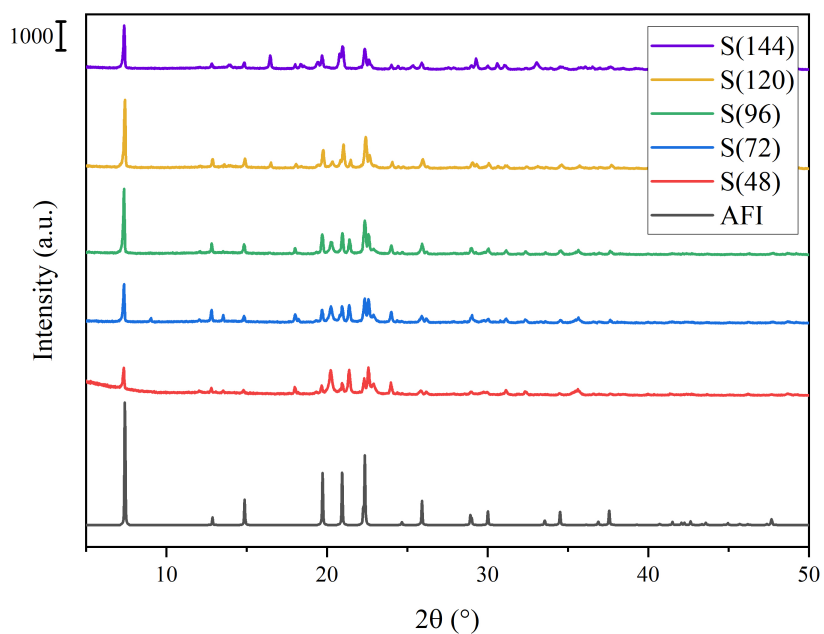

Figure 8.6: Diffractograms of as-prepared samples from experiment investigating crystallisation time, showing sucrose samples.

9   Appendix B - Nitrogen physisorption

Nitrogen physisorption data can be used to classify whether a material is microporous, mesoporous or hierarchical by calculation the Hierarchical Factor [69]. This value can be found using Equation 9.1, and is a product between the relationship of the micropore and total pore volume and the external and BET surface area [69].

$$HF = \left(\frac{V_{micro}}{V_{tot}}\right) \times \left(\frac{S_{ext}}{S_{BET}}\right) \tag{9.1}$$
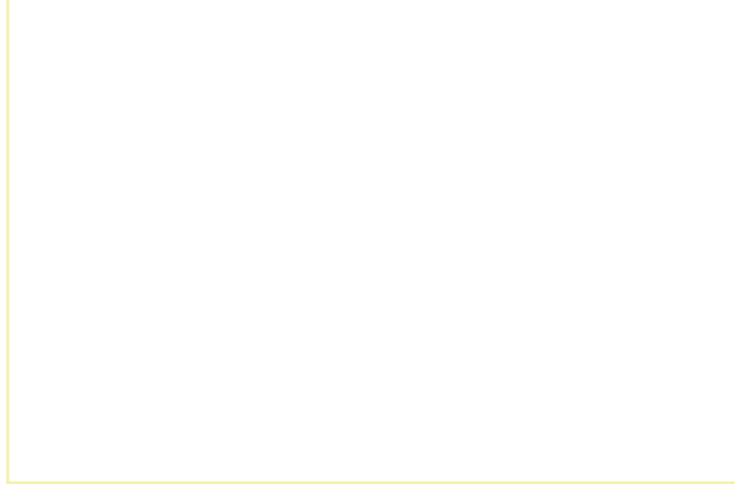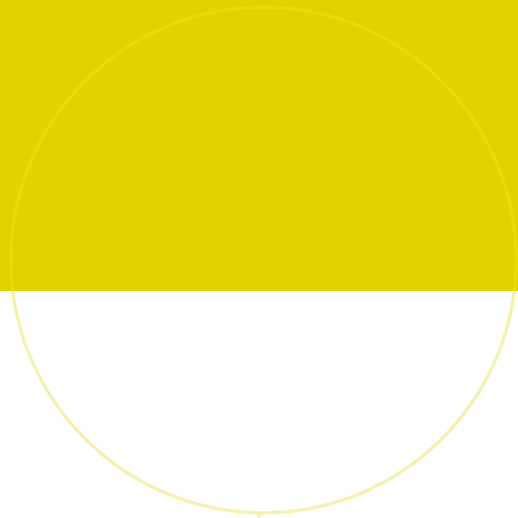
Table 9.1: Data from N_2 physisorption analysis, showing BET, micropore and external surface area, total, microporous and mesoporous volumes and Hierarchical Factor for samples.

Sample name	Surface area (m^2/g)			Pore volume (cm^3/g)			HF
	BET	Micro	Ext	Total	Micro	Meso	
C-SAPO-5	218	161	58	0.12	0.08	0.04	0.19
aG0.025(24)-200	271	202	68	0.16	0.10	0.05	0.17
aG0.05(24)-200	183	122	60	0.11	0.06	0.05	0.19
aG0.1(24)-200	293	241	51	0.17	0.12	0.04	0.13
aG0.2(24)-200	305	247	59	0.18	0.13	0.06	0.13
aG0.3(24)-200	338	270	68	0.20	0.14	0.06	0.14
aS0.025(24)-200	248	200	48	0.14	0.10	0.03	0.15
aS0.05(24)-200	268	214	54	0.15	0.11	0.04	0.15
aS0.1(24)-200	246	198	49	0.15	0.10	0.05	0.14
bG0.025(24)-200	147	102	44	0.18	0.05	0.13	0.09
bS0.025(24/120)-90/200	178	133	45	0.15	0.07	0.08	0.12

10   Appendix C - ICP-MS

Table 10.1: Data from ICP-MS analysis, showing wt.% for aluminium, phosphorus and silicon for each sample analysed.

Sample name	Al wt.%	P wt.%	Si wt.%
C-SAPO-5	16.9	17.8	2.3
aG0.025(24)-200	18.7	20.1	2.8
aG0.05(24)-200	19.9	21.2	3.1
aG0.1(24)-200	19.5	19.8	3.1
aG0.2(24)-200	17.2	18.4	3.4
aG0.3(24)-200	17.4	18.4	2.1
aS0.025(24)-200	16.3	16.8	2.5
aS0.05(24)-200	19.9	21.0	3.2
aS0.1(24)-200	17.5	18.1	3.1
bS0.025-90/200	23.5	26.6	3.0